Title

Experimental Verifi cation of Discretely Variable Compression Braking Control for Heavy Duty Vehicles: Final Report

Authors

Vahidi, Ardalan
Stefanopoulou, Anna G.
Wang, Xiaoyong
et al.

Publication Date

2004-09-01

CALIFORNIA PATH PROGRAM
INSTITUTE OF TRANSPORTATION STUDIES
UNIVERSITY OF CALIFORNIA, BERKELEY

Experimental Verification of Discretely Variable Compression Braking Control for Heavy Duty Vehicles: Final Report

Ardalan Vahidi, Anna G. Stefanopoulou, Xiaoyong Wang, Tsu Chin Tsao

California PATH Research Report
UCB-ITS-PRR-2004-33

This work was performed as part of the California PATH Program of the University of California, in cooperation with the State of California Business, Transportation, and Housing Agency, Department of Transportation; and the United States Department of Transportation, Federal Highway Administration.

Final Report for Task Order 4234

September 2004

ISSN 1055-1425

CALIFORNIA PARTNERS FOR ADVANCED TRANSIT AND HIGHWAYS

Experimental Verification of Discretely Variable Compression Braking Control for Heavy Duty Vehicles: Final Report

Ardalan Vahidi
Anna G. Stefanopoulou
University of Michigan

Xiaoyong Wang
Tsu Chin Tsao
University of California, Los Angeles

TO 4234

Acknowledgments

This work is supported in part by the California Partners for Advanced Transit and Highways (PATH) under TO 4234.

Experimental Verification of Discretely Variable Compression Braking Control for Heavy Duty Vehicles

Ardalan Vahidi Xiaoyong Wang
Anna G. Stefanopoulou Tsu Chin Tsao

Abstract

In the first two chapters of this report, the development of discrete compression brake and transmission models is explained. In the vehicle model development, special efforts have been put in transmission shifting scheduling. Transmission up-shift and down-shift scheduling are separated in the modelling. Hysteresis during shifting is introduced to reduce chattering. A compression brake effect on transmission shifting is identified and considered in the modelling. The new transmission shifting model has been validated through experimental data. The transmission shifting model is combined with the compression brake model and the model of the longitudinal vehicle dynamics for a high-fidelity predictive simulation software tool.

Power-width-modulation (PWM) actuation for brake coordination is proposed to further exploit the capacity of the compression brake and reduce the usage of service brake. Simulation results indicates that the PWM actuation strategy will have the same speed regulation performance as the direct torque split strategy, while the usage of the service brake is significantly reduced, and the compression brake can handle a down slope of -4 when tracking a speed of 56 mile per hour. Simulation results also indicated the importance of vehicle mass and road grade estimation in controller performance. The estimation problem is addressed in detail next.

In the third chapter, a recursive least square scheme with multiple forgetting factors is proposed for on-line estimation of road grade and vehicle mass. The estimated mass and grade can be used to robustify many automatic controllers in conventional or automated heavy-duty vehicles. We demonstrate with measured test data from the July 26-27, 2002 test dates in San Diego, CA, that the proposed scheme estimates mass within 5% of its actual value and tracks grade with good accuracy. The experimental setup, signals, their source and their accuracy are discussed. Issues like lack of persistent excitations in certain parts of the run or difficulties of parameter tracking during gear shift are explained and suggestions to bypass these problems are made.

In the final part of this work, an adaptive model predictive control scheme is designed for speed control of heavy vehicles. The controller coordinates use of compression brakes and service brakes on downhill slopes. The advantage of model predictive control (MPC) scheme over PI design is its ability to explicitly handle the constraints on service brake

and compression command. MPC minimizes use of service brakes based on constrain optimization techniques. Given a perfect model, good performance was obtained in closed-loop. We showed with simulation analysis that model uncertainties due to uncertainty in vehicle mass result in degraded and sometimes poor oscillatory closed-loop response. Unknown road disturbance (grade) was another limiting factor to the performance of the controller. It is shown that accurate estimate of mass is necessary for safe and comfortable operation in closed-loop. Also knowledge of the road grade can improve the results further by contributing in feedforward control. Therefore the estimation method presented in the third chapter of the report is used in parallel with the controller to update the estimates of mass and road grade. We show that adaptation allows robust speed tracking even if initial mass is 300 percent over or underestimated.

Contents

List of Figures

Chapter 1

Vehicle Model for Brake Coordination

1.1 Introduction

The goal of this portion of the project is to investigate the coordination between vehicle service brake and compression brake and minimize the usage of the service brake. Based on the experimental data, we have developed (1) compression brake model; (2) transmission shifting model. We also validated the vehicle dynamic model using the experimental data. We then proposed two strategies for braking force coordination. A PI controller is tuned to simulate the speed regulation performance of the whole system and the results of each braking coordination strategy are compared. Finally we implemented online road grade and vehicle mass estimation and used grade and mass feed forward to improve speed tracking performance.

1.2 Compression brake model

This model has been presented in the previous annual report. The result is included in this report to make it complete and self-contained.

Compression brake model:

$$\mathrm{T_{high}} = 0.0003\omega^2 - 0.0347\omega + 162.84$$

$$\mathrm{T_{low}} = 0.2352\omega - 1.8568$$

Where ω is engine speed in rpm, $\mathrm{T_{high}}$ is high-mode compression torque in Nm; $\mathrm{T_{low}}$ is low-mode compression torque in Nm.

1.3 Transmission shifting schedule

As we presented in the most recent formal PATH meeting, further refinement of the transmission shifting schedule model was one of our future tasks. The transmission sits between the engine and the driving wheels. It is the most important system in the whole driveline. This report is focused on the recent effort we put on the transmission shifting schedule model.

In the modeling process, we are inspecting the data collected on July 27 and 28, 2002, and figure out the factors that determines the shifting process. Then a coarse table, which will map the region of values of the factors to the gear, is constructed. Refining this table with more data files and finer resolution, a shifting schedule is produced. By running this schedule with the same vehicle signals and plotting the gear shifting process, we are able to look at the difference between the predicted shifting and the actual shifting. This is what was done before. While the model at least provide us a way to determine gear shifting, it has several unfavorable aspects: (1) It generates shifting bounce under some situations, (2) It doesn't cooperate with the compression brake which will set the top gear to 4 upon application, (3) The amount of undesired shifting are considerable.

In our current effort, the experiment data are examined more closely, and new strategies are applied to improve the basic model.

1.3.1 Previous Results

In automatic transmission, the gear selection is mainly affected by the vehicle speed (transmission output shaft angular speed) and the acceleration pedal position. This is realized in transmission operation as following: a speed governor at the output shaft is monitoring the output speed and generating a corresponding shifting pressure in the shifting cylinder. This pressure is also regulated by the acceleration pedal position. Deeper position will delay the shifting from lower gear to next higher gear to maintain the traction force for accelerating the vehicle or climbing hills. As we plot the output shaft speed, the pedal position and the current gear, the relationship is obvious (**Figure 1.1**).

A shifting table is constructed from this data plot. This 2-D lookup map takes the transmission output shaft speed and acceleration pedal position as its input parameters and interpolates to get the closest gear (**Figure 1.2**).

The shifting model improves our vehicle dynamic model in the sense that we no longer need to assume a constant gear ration. To give a sense how close the model is to real situation, the shifting model is used to generate the shifting prediction under the same combination of transmission output shaft speed and acceleration pedal position as collected in an experiment run. The predicted shifting and the actual one are graphed in the same plot (**Figure 1.3**).

Since there is no sharp delimitation between different regions, and the overlaps between some gears (for example, 5 and 6) are very large (**Figure 1.1**). These cause several problems. Among

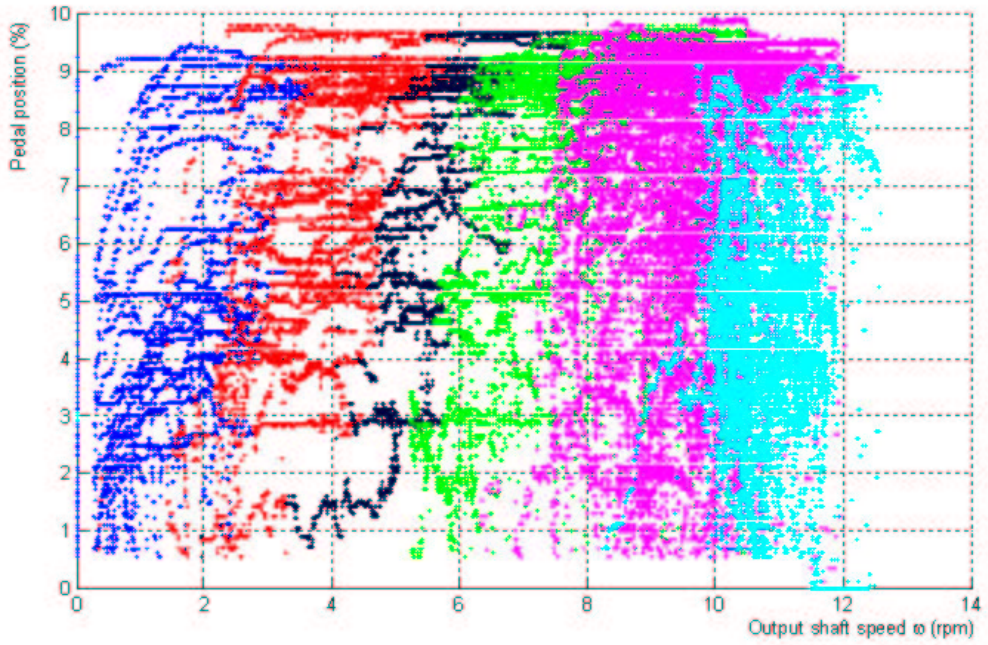

Figure 1.1: Shifting Data - Experiment: Blue-Gear 1; Red-Gear 2; Black-Gear 3; Green-Gear 4; Magenta-Gear5; Light blue-Gear6

them are shifting bounce, incorrect shifting timing, unexpected shifting and missed shifting, as we have already seen in **Figure 1.3**.

1.3.2 New Strategies

To improve the accuracy of the transmission shifting model, we can only turn back to the experiment data and give it a much closer examination. As more efforts are put in, the following facts emerge: (1) The application of compression brake downshifts the gear to 4 immediately if it is above 4, (2) When the vehicle is decelerating (braking), the pedal position is 0, no driver would touch the pedal during this period, (3) the critical points where downshift and upshifting happen are different, which form a shifting hysteresis for each gear.

To apply these facts to our model, we adopt the following strategies. (1) If the vehicle is accelerating, the shifting schedule assumes a 2-D lookup table form, constructed from the vehicle data in acceleration. (2) If the vehicle is braking, the shifting schedule assumes a 1-D lookup table, which takes the transmission output speed as its only input parameter. The map is constructed from the vehicle data in deceleration. (3) If compression brake is applied during braking, the gear downshifts to 4 directly if it is above 4 upon the application. (5) For adjacent gears, use different critical shift conditions to model shift hysteresis.

The overlaps between gears in **Figure 1.1** are largely caused by different shifting conditions in acceleration and deceleration. By separating them and modeling the hysteresis for each gear pair,

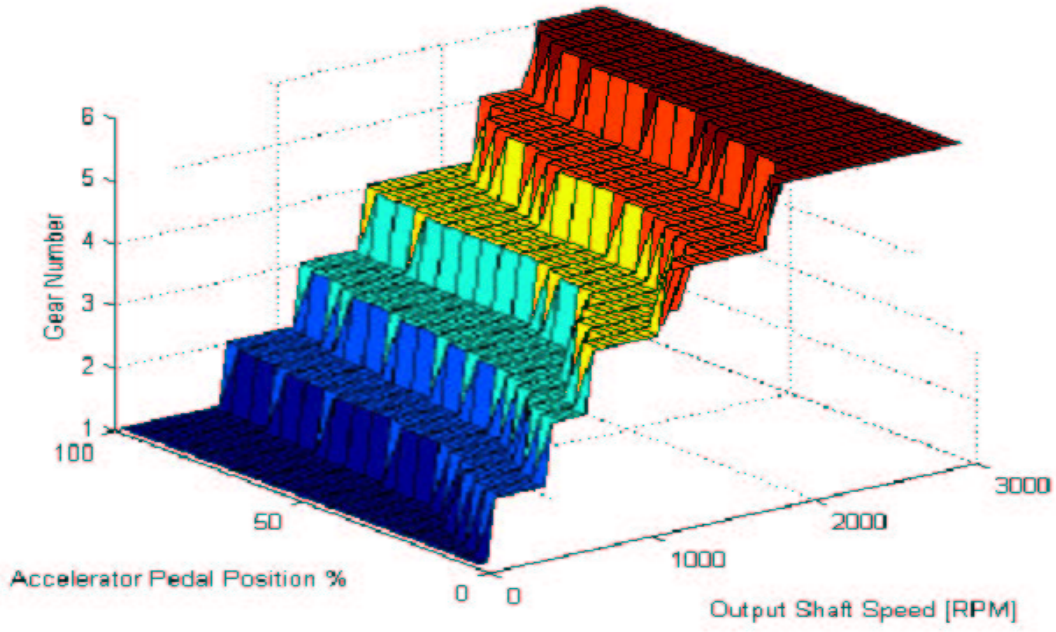

Figure 1.2: Part of acceleration shift schedule

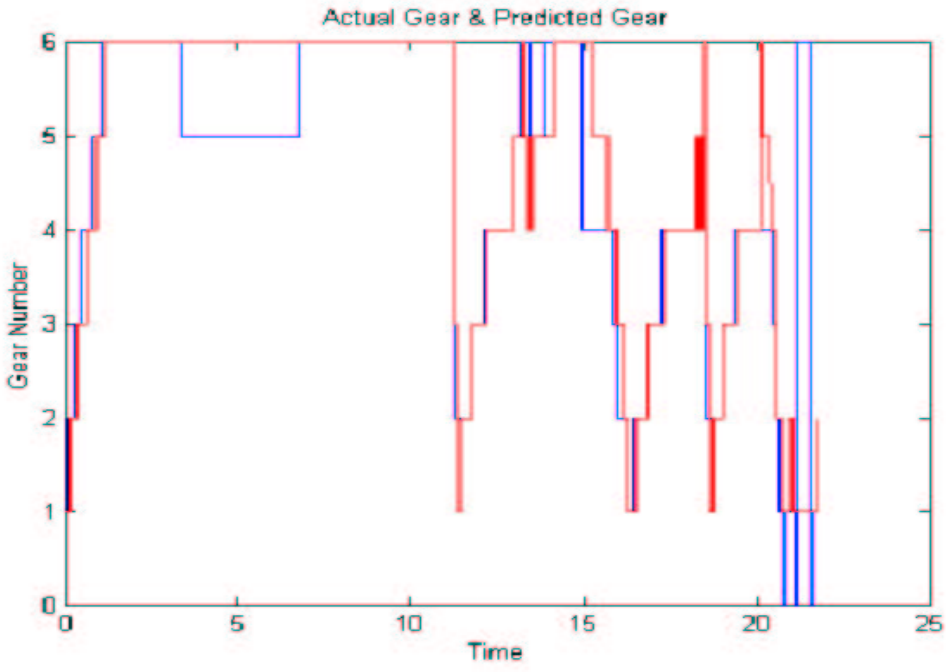

Figure 1.3: Predicted and actual shifting process

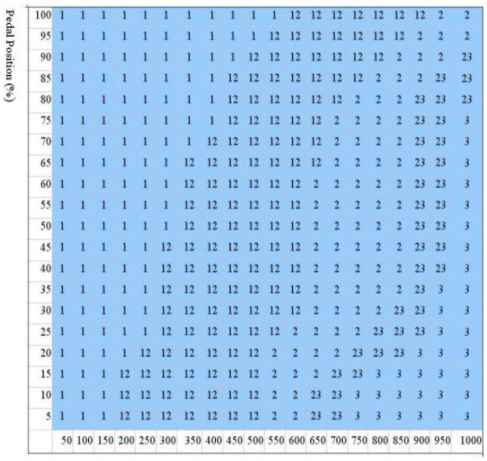

Figure 1.4: Part of acceleration shift schedule

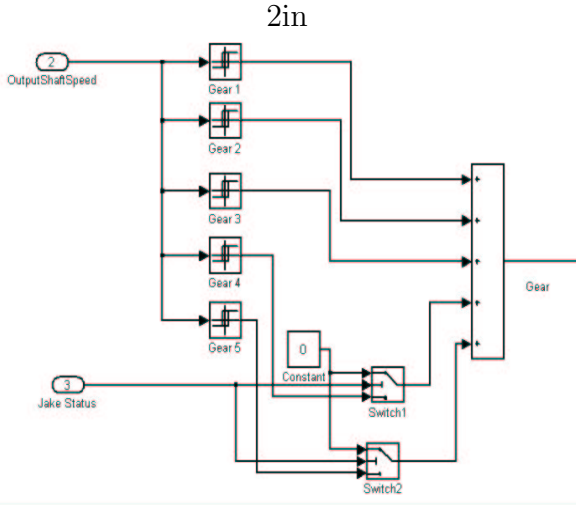

Figure 1.5: Deceleration shifting implementation

the shifting bounce problem will be alleviated. As byproducts, the occurrences of unexpected and missed shiftings, the offset of shifting timing will be reduced. The top gear restriction logic imposed by compression brake makes the model even closer to the actual vehicle.

Acceleration Shifting Model

The table in **Figure 1.4** is a part of the shifting schedule for acceleration (from 50 - 1000 RPM). The table is constructed from the accelerating data exacted from the experiment data files. This model uses the '12', '23', '34', '45', '56' to indicate that in the corresponding region, the gear may be either one of the two numbers. The logic used to determine which gear to choose is that if the selected gear is the same as the previous gear. That means, for example, if the gear goes from '1' to arrive '12' zone, the selected gear is 1. But if the gear goes from '2' to '12' zone, the selected gear is 2. This is nothing but the acceleration gear shifting hysteresis.

Deceleration Shifting Model

In deceleration, the gear is a function of transmission output shaft speed only. The hysteresis is easily implemented in MATLAB using its hysteresis module (**Figure 1.5**). Compression brake (Jake brake) status is used to restrict the top gear to 4. The difficulty in this model lies in how to get the hysteresis of each gearshift. It requires extracting the braking data from the experiment data files and finding the best numbers to fit for each gear.

1.3.3 Validation

Again, the new model is inspected using the experiment data and its prediction of gear shifting is compared with the actual gearshift in that experiment run (**Figure 1.6**). From this result, the shifting process predicted by the model is much closer to the actual shifting process. The shifting

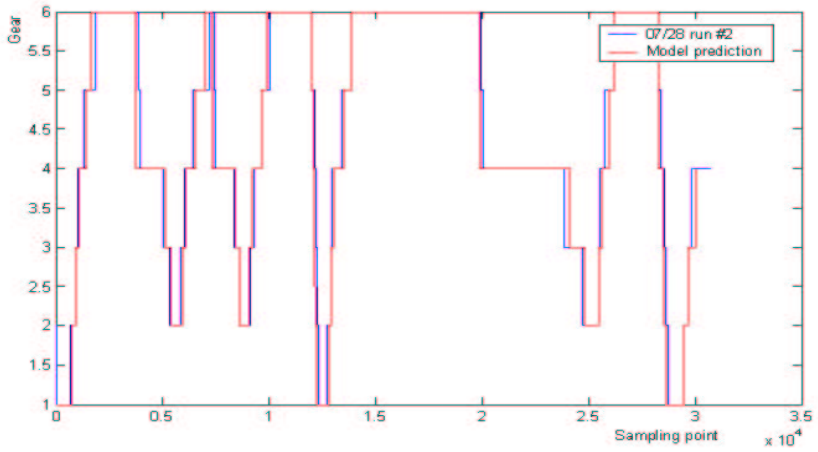

(a) *Example1*

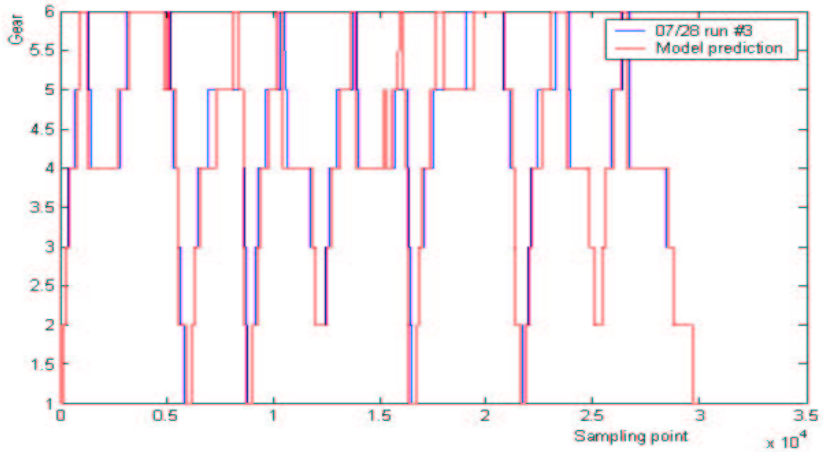

(b) *Example2*

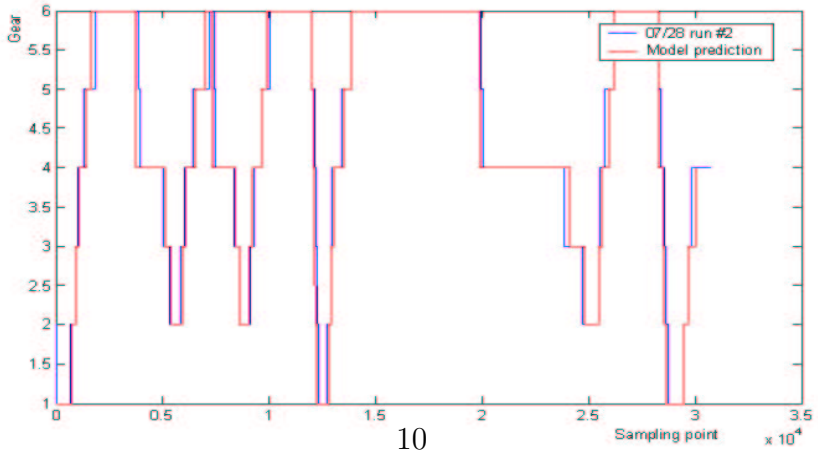

(c) *Example3*

bounce doesn't show up in this run; the unexpected and missed shifting times are reduced. The timing offset is very small. All of these provide a sense that the new model is much better than the previous one.

1.4 Vehicle longitudinal dynamic model in braking

The compression brake and transmission map were added to an existing vehicle dynamic model previously developed in [29]. The acceleration of the vehicle is determined by the engine torque, road grade, rolling resistance, wind drag and vehicle braking force. In characterization of the vehicle braking behavior, the engine traction torque will be assumed to be zero. But the engine may generate braking torque if engine compression brake is engaged. Using experimental data, we identified the wind drag coefficient and the rolling resistance coefficient [41]. The vehicle longitudinal dynamic model is give by:

$$\dot{v} = \frac{1}{M_{eff}}(\frac{T_{dr} r_g r_d}{r_w} - g\sin\beta - \mu g\cos\beta - \frac{1}{2}C_d A_v v^2 - F_{sb})$$

Where

v: Vehicle speed in m/s

M_{eff}: Vehicle effective mass in Kg

T_{dr}: Driveline torque in $N \cdot m$

r_g: Transmission gear ratio, scalar

r_d: Differential gear ratio, constant scalar

r_w: Driving wheel effective radius in m

g: Gravational acceleration, constant, $9.81 m/s^2$

β: Road grade in rad, positive if up slope, negative if downslope

μ: Rolling resistance coefficient, constant scalar

C_d: Vehicle wind drag in $N \cdot s^2/m^4, constant$

A_v: Vehicle frontal area in m^2, constant

F_{sb}: Service brake force in N

1.5 Conclusion

In this chapter, a vehicle dynamic model for brake coordination is established. By introducing hysteresis and separating the up-shifting and down-shifting maps, the transmission shifting schedule is substantially improved. The experimental data is exploited extensively to determine the thresholds of each hysteresis.

Chapter 2

Brake Coordination

2.1 Brake coordination strategies

The coordination between service brake and engine compression brake is the main focus of this project. The ultimate goal is to minimize the usage of service brake while regulating the vehicle speed.In speed tracking, the desired braking torque (force) is calculated by a controller. There are three braking sources in the truck: wheel service brake, engine compression brake and transmission retarder. Then how to allocate this torque (force) to different braking sources? We only consider the coordination between compression brake and service brake. A new allocation strategy is proposed in this chapter and compared with the direct torque split strategy [2]. We begin by explaining how direct torque split strategy works.

2.1.1 Direct torque split

At each time, the compression brake capacity T_{high}, T_{low}(the torque produced) for high mode and low mode are calculated respectively, according to the compression braking model (1) and (2). The braking torque command T_{cmd} (the desired torque calculated by the controller) is then compared with T_{high}, T_{low}:

If $T_{cmd} < T_{low}$, then $T_{braking} = T_{service}$;

Else if $T_{low} \leq T_{cmd} \leq T_{high}$, then $T_{service} = T_{braking} - T_{low}, T_{comp} = T_{low}$;

Else $T_{service} = T_{braking} - T_{high}, T_{comp} = T_{high}$.

The algorithm assumes that the service brake system is able to generate enough braking torque if needed.

The latter two cases represent the"splitting torques" scenario where the torque required is split between the compression brake (in low or high mode) and the service brake. The outputs of the braking algorithm, and are then given as inputs to the vehicle dynamics model.

Adding the braking algorithm created some problems for our simulation. The largest problem we ran into was extreme chattering in the system whenever the algorithm had to decide between

whether to use T_{high} or T_{low} or whether to use the compression brake at all. This can be shown through a numerical example. Say the engine is at 1700 RPM and $T_{braking} = 400$. The algorithm determines that 398.13 Nm can be supplied via the low mode of the compression brake and turns it on and the remaining 1.87 Nm is supplied by the service brake. This braking slows the vehicle down and then in subsequent times through the loop the braking torque required is less and less and eventually $T_{braking} = T_{low}$. When this happens the algorithm turns the compression brake on and all of the required braking torque is supplied by the compression brake. But the next time through the loop $T_{braking}$ is slightly less than T_{low} and the compression brake is not used. This chattering between turning the compression brake on and off stalls the simulation because it cannot come up with a clear-cut decision. To avert this issue we added a "backlash" as well as a "dead zone" block from MATLAB. The dead zone block allows you to create a dead zone of values for which if the input falls in that zone the output is zero (the controller does nothing). Adding the dead zone made it so that the system would not react to such small differences and therefore not chatter when the required braking torque value approaches the threshold between turning the compression brake on or off or deciding to be in high or low mode. The "backlash" block acts as a hysterisis and allowed us to set a "bandwidth" that allows an amount of play in the system.

2.1.2 Generate compression brake torque by PWM actuation

One drawback of above strategy is that even if the desired torque is within the capacity range of the compression brake, the actual brake torque is either totally or partially generated by the service brake. This is determined by the discrete nature of the torque that the engine compression brake can generate at a given engine speed. To address this issue, we proposed a different allocation method. The idea beneath this method is that a continuous varying torque effect can be simulated by frequently switching on or off the compression brake. The terminology to describe this kind of actuation is call pulse width modulation (PWM). For each period, the average torque is determined by the pulse width (duty cycle).

The PWM frequency should be well chosen. Generally speaking, the higher the switching frequency, the smaller the output torque pulsating. The compression brake system response time will set the upper limit of the PWM frequency. Some other issues should also be considered, such as system life and reliability if switching at high frequency. In our computer simulation, we set the frequency to be 1 Hz.

Accordingly, we discretized the controller with sampling time $T = 1s$. The controller calculates the braking torque command at each sampling point and this command is fed into the PWM generator to produce the switching signal for the compression brake. The algorithm is:

If $T_{cmd} \leq T_{low}$, then $T_{brake} = T_{low}$ modulated by pulse width $W = \frac{T_{cmd}}{T_{low}}$;

Else if $T_{cmd} \leq T_{high}$, then $T_{brake} = T_{high}$ modulated by pulse width $W = \frac{T_{cmd}}{T_{high}}$;

Else, $T_{brake} = T_{high} + T_{service} = T_{cmd}$ with pulse width $W = 1$

By looking at the algorithm, when the command torque is less than the compression brake capacity, the engine compression brake will generate all the braking torque and the service

brake is not involved. The usage of the service brake is reduced, compared with the direct torque split method. We should see this in simulation later on.

2.2 PI controller

For the vehicle speed tracking, the system is a first order system if we treat wind drag and grade-caused forces as disturbances to the system. In this case, a PI controller will be good enough to perform the task. The controller parameters are tuned by simulation. In PWM actuation case, the controller is discretized using sampling time 1 to implement the algorithm.

2.3 Simulation results

To see if the coordination between the compression brake and the service brake works, and how the designed scheme can help to minimize the usage of service brake, and what the over all system tracking performance would be, a SIMULINK model is built based on the identified vehicle compression brake model, transmission map, vehicle dynamic model, and control and brake coordination algorithms.

2.3.1 Simulation setup

We are only dealing with the vehicle braking performance, so the simulation assumes a down slope road, and during the whole process the engine doesn't generate traction torque. The only force that accelerates the vehicle is due to the negative road grade. The road profile is generated by computer program with piecewise constant grade (**Figure 2.1** & **Figure 2.2**). The maximum grade is -6 . The road is made of 11 sections, with a constant grade for each section. Each section has a length from 500 meters to 2000 meters. Since the grade of most freeways is less than 6 % (6), this choice of the grades is reasonable.

The simulation starts with vehicle speed $25m/s$ (56 $mile/h$). The reference speed is set to be $25m/s$ (56 $mile/h$). On most freeways the speed limit for trucks on slopes is 55 $mile/h$. The total vehicle mass is $2.59 \times 10^4 Kg$ with payload $1.18 \times 10^4 Kg$.

2.3.2 Tracking performance: Direct torque split vs. PWM

The speed tracking performance can be directly seen from the simulation plots (**Figure 2.3** & **Figure 2.4**). Both configurations result in very small tracking errors. This shows that the PI controller is good enough for speed regulation and different brake coordination schemes have little effects on speed tracking. The maximum speed tracking error is less than 1.5 $mile/h$.

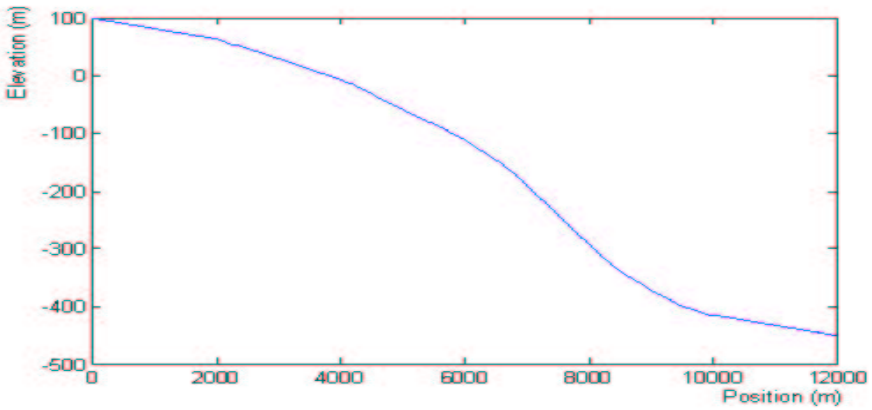

Figure 2.1: Road profile

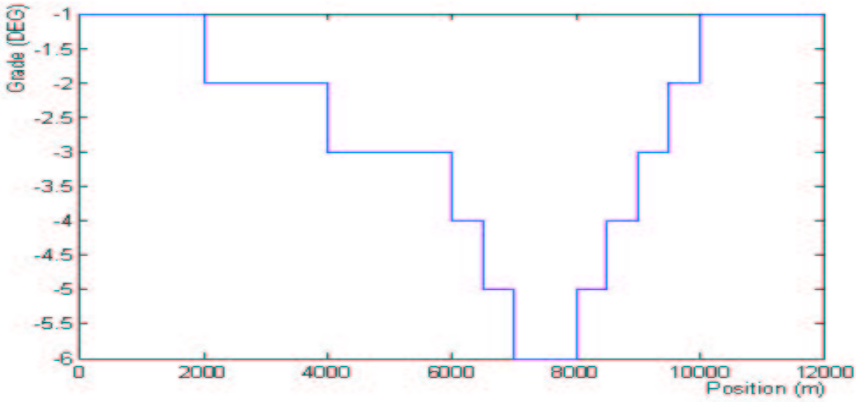

Figure 2.2: Road grade

2.3.3 Brake coordination: Direct torque split vs. PWM

The service brake usage of each brake coordination scheme in the simulation is plotted in **Figure 2.5** and **Figure 2.6**. The compression brake usage of each scheme is plotted in **Figure 2.7** and **Figure 2.8**. The red line in each plot represents the command brake force. The blue lines are the brake forces generated by corresponding sources.

In the plots, the differences between the direct torque split scheme and the PWM scheme appear when the torque command is less than the current available compression brake force (low mode or high mode). From 0 to about 60 s, the braking force command is less than the compression brake force capacity of low mode. The direct torque scheme generates the braking force by service brake (**Figure 2.5**), and the compression brake is not applied (**Figure 2.7**); The PWM actuation scheme generates the braking force by compression brake (**Figure 2.8**), and the service brake is not applied (**Figure 2.6**). From 60 s to 240 s, the command lies between the low mode capacity and the high mode capacity. The direct torque split scheme engages the compression brake in low mode and picks up the remaining braking force by the service brake; The PWM

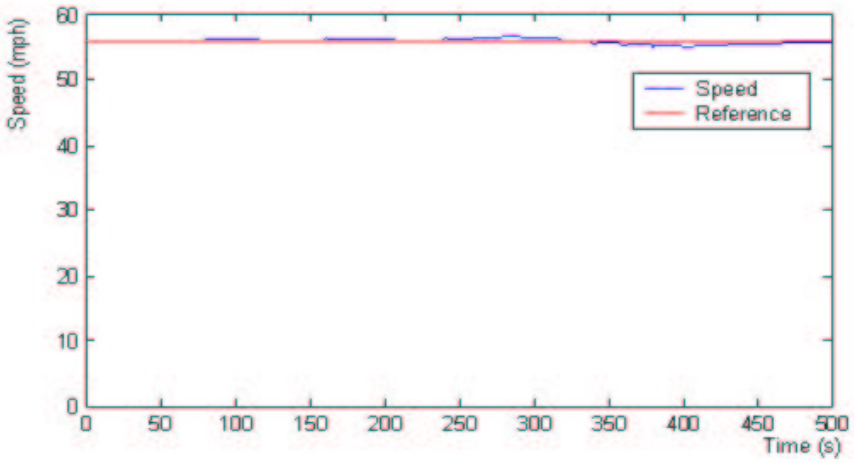

Figure 2.3: Speed tracking: Direct torque split

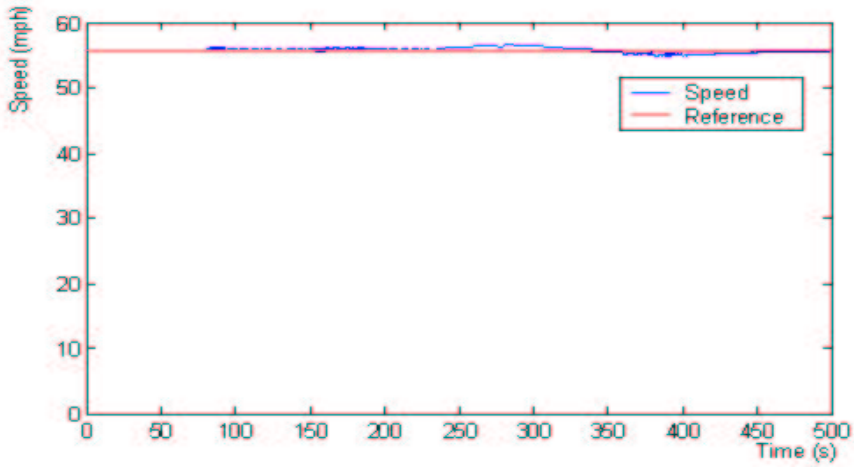

Figure 2.4: Speed Tracking: PWM actuation

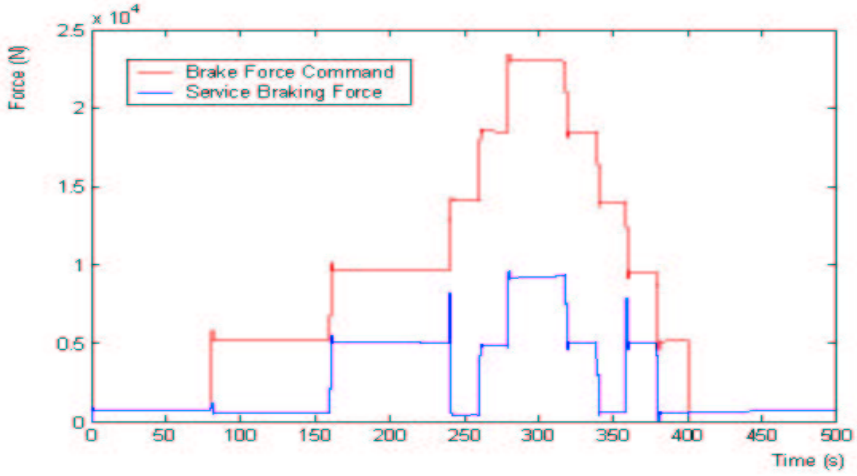

Figure 2.5: Service brake usage: Direct torque split

actuation scheme generates the braking force only by the compression brake. From 240 s to 360 s the compression brake is engaged in high mode in either scheme because the command is greater than high mode
capacity. Similar analysis can be done to the rest of the simulation. The usage of service brake is reduced significantly in the PWM actuation scheme compared with the direct torque split scheme. The simulations also show that the compression brake can handle road grade up to -4 . But if the driver intentionally shifts down to gear 3 or even lower gear, more braking force can be generated to handle higher grades. Also if the payload is reduced, then less braking force is needed and the compression brake can handle higher grades.

2.4 Speed tracking with parameter estimation

The road grade affects the acceleration of the vehicle in two ways: changing the tangent force to drag or accelerate the vehicle and changing the rolling friction force by changing the normal force. If we take the road grade as a disturbance to the vehicle system, the vehicle speed tracking performance will be improved if we can somehow cancel the disturbance effect. This can be done by road grade and vehicle mass feed forward. For each single trip, vehicle mass can be taken as constant. The road grade is obtained either by GPS (Global Positioning System) with GIS (Geography Information System) database or by online estimation. We implemented an online estimation algorithm.

2.4.1 Algorithm

Before apply the standard RLS (Recursive Least Square), we can write the system as:

$$\dot{v} = -(F_{brake} + K_{aero}v^2)\frac{1}{M} + \frac{-g}{\cos\beta_\mu}\sin(\beta + \beta_\mu)$$

$$\beta_\mu = \arctan\mu$$

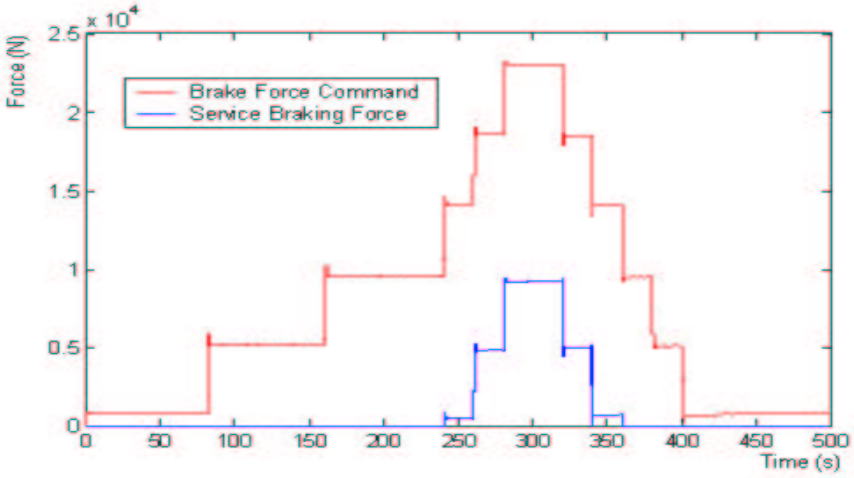

Figure 2.6: Service brake usage: PWM actuation

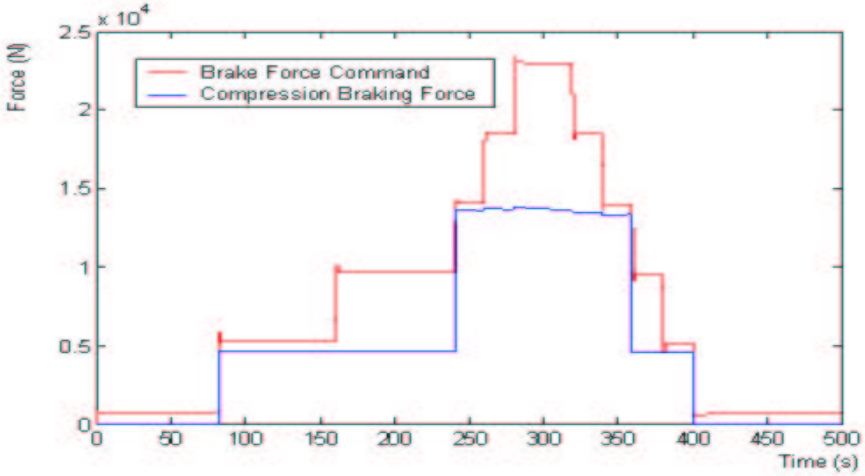

Figure 2.7: Compression brake usage: Direct torque split

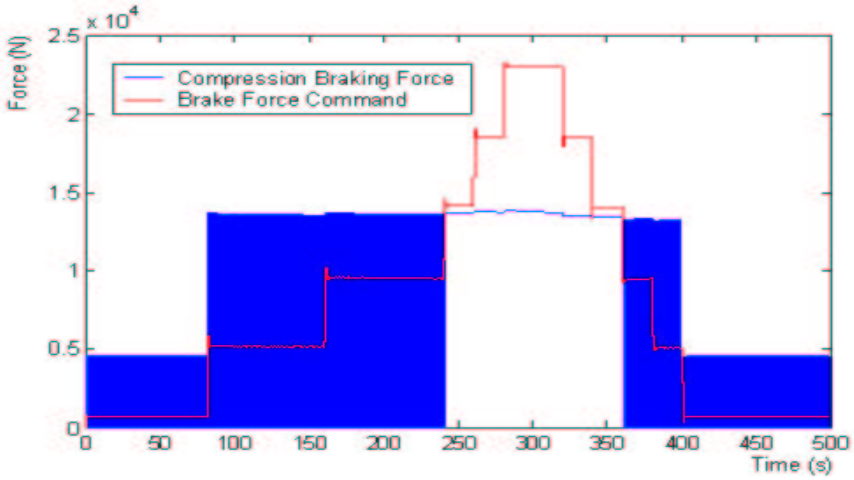

Figure 2.8: Compression brake usage: PWM actuation

Where μ is the rolling friction coefficient

So the estimation model is:

$$y = \phi_1\theta_1 + \phi_2\theta_2$$
$$\theta_1 = \frac{1}{M}$$
$$\theta_2 = \sin(\beta + \beta_\mu)$$
$$\phi_1 = -(F_{brake} + K_{aero}v^2)$$
$$\phi_2 = -\frac{g}{\cos\beta_\mu}$$

The RLS algorithm with forgetting is given by:

$$\hat{\theta}(k) = \hat{\theta}(k-1) + L(k)(y(k) - \varphi(k)\hat{\theta}(k-1))$$
$$L(k) = \frac{P(k-1)\varphi(k)}{\lambda + \varphi(k)^T P(k-1)\varphi(k)}$$
$$P(k) = \frac{(I - L(k))\varphi(k)^T P(k-1)}{\lambda}$$

2.4.2 Estimation results

The estimated grade and mass are plotted in **Figure 2.9** and **Figure 2.10**. A single forgetting factor of 0.8 is used in the estimation. Since the road grade is not constant but piecewise constant, the forgetting factor is indispensable. The forgetting factor has the effect to put more weight on the recent data, and less weight on the old data, or 'forget' the history. From the plots, during grade transition there are sharp spikes in both grade and mass estimation. The forgetting factor then brings the estimated data to their nominal values.

The estimated data are very close to their actual values except at the grade transition points. These spikes are due to the quick transition of the grade. It is imaginable that if the grade is not piecewise constant but an arbitrary smooth function, there will be more but smaller spikes.

If the estimated mass and grade data are not clean, the introduction of the mass and grade feed forward may deteriorate the system tracking performance. One may want to filter the estimated data since the road grade and vehicle mass has a priori known ranges. The other RLS algorithms, such as RLS with multiple forgetting factors may be exploited to deal with this problem [40]. More details are given in the next section of this report.

2.5 User interface

A user interface is developed for simulation purpose (**Figure 2.11**). Vehicle model details are encapsulated under the interface. It provides a convenient way to tune controller parameters through run-by-run trial. It could be integrated with vehicle display unit to monitor brake coordination status.

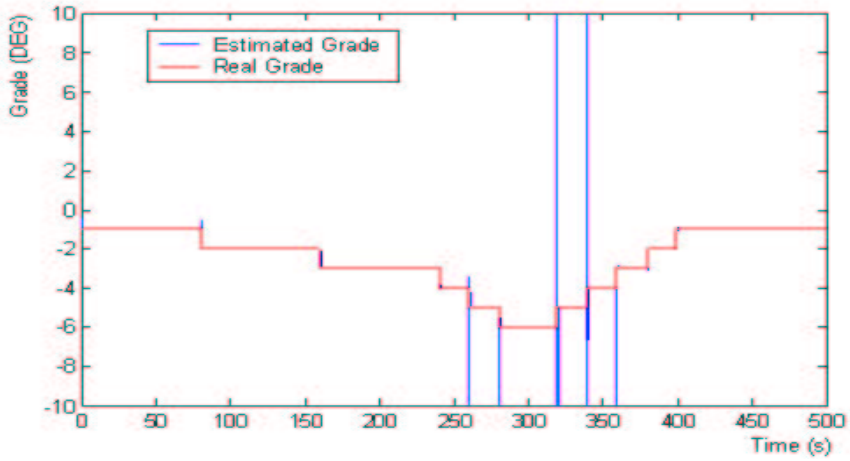

Figure 2.9: Grade estimation

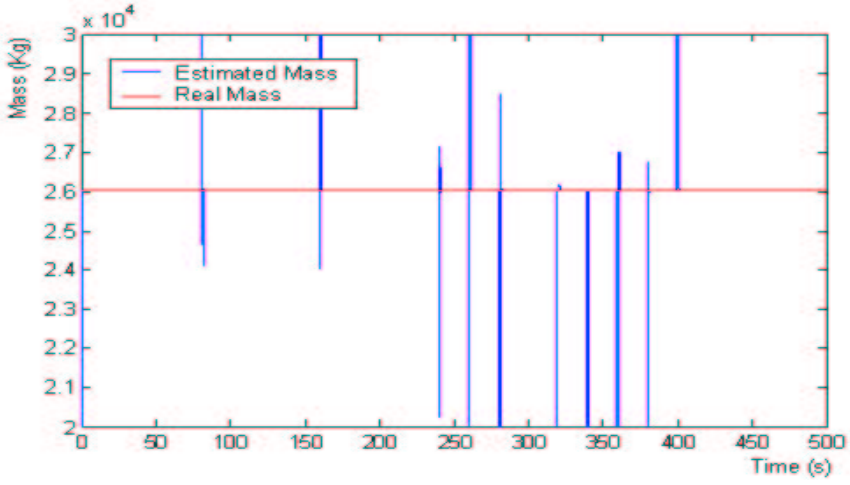

Figure 2.10: Mass estimation

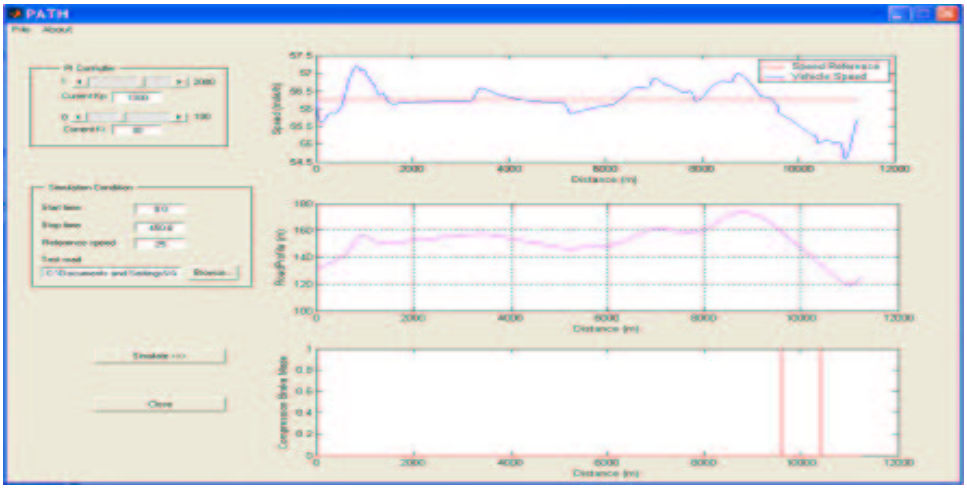

Figure 2.11: User interface

2.6 Conclusion

In this chapter, a new brake coordination strategy is proposed and compared with the previous strategy. The proposed PWM actuation strategy reduces the service brake usage much further than the direct torque split strategy. A convenient user interface is developed for simulation purpose. Online grade and vehicle mass estimation is implemented and simulation results indicate that more needs to be done to improve the estimation performance. The estimation problem is addressed in detail in the next section of the report.

Chapter 3

Parameter Estimation

3.1 Introduction

In vehicle control, many control decisions can be improved if the unknown parameters of the vehicle model can be estimated. Weight of the vehicle, coefficient of rolling resistance, and drag coefficient are examples of unknown parameters. Road grade is a major source of external loading for heavy vehicle longitudinal dynamics and is normally unknown. Both mass and grade are found to be critical in section 2.4. The mass of a heavy duty vehicle can vary as much as 400% depending on the load it carries. Mild grades for passenger vehicles, are serious loadings for heavy vehicles.

Due to their importance, this section is devoted to development and comparison of on-line parameter estimation algorithms. An algorithm for simultaneous estimation of mass and grade that takes into account realistic rates of change for each parameter is developed. The algorithm can be integrated with a speed tracking (or regulation) controller. It can also be used for various other vehicle controllers. Specifically, an anti-lock brake controller relies on an estimate of mass and road grade for calculating vehicle's cruise speed which is necessary for estimation of wheel slip. In longitudinal control of platoons of mixed vehicles, knowledge of the participating vehicle mass and road grade is necessary for avoiding issuing infeasible acceleration and braking commands [4]. Moreover, mass estimation is essential to the engine control unit (ECU) for reduced emission, and to transmission control for reduced gear hunting. The closed loop experiments performed by Yanakiev et al. [44] indicate that the longitudinal controllers with fixed gains have limited capability in handling large parameter variations of an HDV. Therefore it is necessary to use an adaptive control approach with an implicit or explicit online estimation scheme for estimation of unknown vehicle parameters.

Examples of adaptive controllers for vehicle control applications can be found in the work by Liubakka et al. [23], Ioannou et al. [17], and Oda et al [30]. Yanakiev et al. [45, 46] have developed an adaptive controller for longitudinal control of an HDV using direct adaptation of PIQ controller gains. Recently, Druzhinina et al. [12] have developed an adaptive control scheme for longitudinal control of HDV's. Within this scheme they provided simultaneous mass and road grade estimation. They demonstrated convergence in estimates for constant mass and piecewise constant grade. This method is an indirect estimation method since estimation is achieved in closed-loop and as a by-product of a control scheme.

As HDV automation is increasing, there are more controllers that could benefit from on-line estimation of the vehicle mass and road grade. Moreover many times estimates independent of a controller are required. In other words a direct estimation scheme is more appealing. The proposed schemes for direct estimation of vehicle parameters, particularly mass and grade can in general be classified in two categories: sensor-based and model-based methods. In sensor based methods some type of extra sensor is used on the vehicle to facilitate estimation of one or more parameters. Model-based schemes use a model of the vehicle and data like engine torque, vehicle speed, engine speed and gear ratio which are available through the CanBus to estimate the unknown parameters. Since longitudinal dynamics of the vehicle depends on both mass and grade, knowing one will facilitate estimation of the other. Therefore some suggest estimating the grade which is in general time varying with some type of sensor and then estimating the mass with conventional parameter-adaptive algorithms [17, 43]. Bae et al. [5] use GPS readings to obtain road elevation and calculate the grade using the measured elevations. With the grade known, they estimate the mass with a simple least square method based on the longitudinal dynamics equation. In [31] using an on-board accelerometer is proposed for grade estimation. The mass is then estimated based on a good approximations of the grade.

A model-based method can provide a cheap alternative in estimation or it can be used along with a sensor-based scheme to provide some redundancy. One approach [15] which has been patented and has been used in industry is estimation of mass based on the velocity drop during a gearshift. The idea is that since the gearshift period is short, the road load can be rendered constant. The change in velocity before and during gearshift can be used to calculate an estimate for the mass based on the longitudinal dynamics equation. However based on a fair amount of trial, we observed that the velocity drop is normally minor during a gearshift and this limits the accuracy of the method due to the small signal-to-noise ratio. Besides, this approach does not address estimation of the grade.

In the rest of this chapter a direct approach for simultaneous estimation of mass and time-varying grade is pursued. We first formulate vehicle longitudinal dynamics and explain experimental setups and validation of longitudinal model. We then investigate implementation of a recursive least square (RLS) method for simultaneous online mass and grade estimation. We briefly discuss the recursive least square scheme for time varying parameters and review some key papers that address the subject. The difficulty of the popular RLS with single forgetting is discussed next. For estimation of multiple parameters which vary with different rates, RLS with vector-type forgetting is previously proposed in a few papers. We analyze this approach and propose an ad-hoc modification of the update law for the gain in the RLS scheme. We demonstrate, with both simulated and test data, that incorporating two distinct forgetting factors is effective in resolving the difficulties in estimating mass and time-varying grade. The experimental setup and particular issues with experimental data are also discussed.

3.2 Vehicle Longitudinal Dynamics

Our estimation approach is a model based approach. That is, we rely on a physical model of vehicle's longitudinal dynamics and use this model and the data that is recorded from the vehicle's CanBus for estimating mass and grade and possibly other unknown parameters which affect vehicle's longitudinal motion. Therefore we first formulate the vehicle longitudinal dy-

namics equations which are a bit redundant with section 1.4 but are added here to facilitate the notation.

A vehicle's acceleration is a result of combination of engine and braking torques and the road loads on the vehicle. When the torque convertor and the driveline are fully engaged we can assume that all the torque from the engine is passed to the wheel. Further assuming that there is no wheel slip, which is a good assumption for most part of the motion, the longitudinal dynamics can be presented in the following simple form:

$$M\dot{v} = \frac{T_e - J_e\dot{\omega}}{r_g} - F_{fb} - F_{aero} - F_{grade} \tag{3.1}$$

In this equation M is the total mass of the vehicle, v is the forward speed and ω is rotational engine speed. T_e is the engine torque at the flywheel. If engine is in fuelling mode the torque is positive and if it is in the compression braking mode the torque is negative. If the transmission and the torque convertor are fully engaged then most of the torque is passed to the wheels as assumed in the above equation. To model the possible torque losses, engine torque can be scaled down by a coefficient of efficiency. J_e is the powertrain inertia and therefore the term $J_e\dot{\omega}$ represents the portion of torque spent on rotating the powertrain. r_g is the wheel radius divided by total gear ratio:

$$r_g = \frac{r_w}{g_d g_f}$$

where r_w is the wheel radius, g_d is the gear ratio and g_f is the final drive ratio. F_{fb} is the generated friction brake (service brake) force at the wheels. The force due to aerodynamic resistance is given by

$$F_{aero} = \frac{1}{2}C_d\rho A v^2$$

where C_d is the drag coefficient, ρ is air density and A is frontal area of the vehicle. F_{grade} describes the combined force due to road grade (β) and the rolling resistance of the road (μ). It is given by

$$F_{grade} = Mg(\mu\cos\beta + \sin\beta),$$

where g is the gravity constant. Here $\beta = 0$ corresponds to no inclination, $\beta > 0$ corresponds to uphill grade and $\beta < 0$ represents downhill. Eq. (4.2) is valid when the wheels do not have considerable slip.

We are interested in using this equation along with the data obtained from vehicle's CanBus for online estimation of mass and grade. In section 3.3 signal measurement and identification of model parameters are explained.

Equation (4.2) can be rearranged so that mass and grade are separated into two terms:

$$\dot{v} = (\frac{T_e - J_e\dot{\omega}}{r_g} - F_{fb} - F_{aero})\frac{1}{M} - \frac{g}{\cos(\beta_\mu)}\sin(\beta + \beta_\mu) \tag{3.2}$$

where $\tan(\beta_\mu) = \mu$. We can rewrite Eq. (3.2) in the following linear parametric form,

$$y = \phi^T\theta,\ \phi = [\phi_1, \phi_2]^T\ \theta = [\theta_1, \theta_2]^T \tag{3.3}$$

Where

$$\theta = [\theta_1, \theta_2]^T = [\frac{1}{M},\ \sin(\beta + \beta_\mu)]^T$$

are the unknown parameters of the model, which we try to estimate and

$$y = \dot{v},\ \phi_1 = \frac{T_e - J_e\dot{\omega}}{r_g} - F_{fb} - F_{aero},\ \phi_2 = -\frac{g}{\cos(\beta_\mu)}$$

can be calculated based on measured signals and known variables.

Had the parameters θ_1 and θ_2 been constant, a simple recursive algorithm, like recursive least squares, could have been used for estimation. However while θ_1 depends only on mass and is constant, the parameter θ_2 is in general time-varying. Tracking time-varying parameters needs provisions that we directly address later in this chapter.

3.3 Experimental Setup

We planned experiments on the PATH Freightliner truckH. The signals are measured through different interfaces. The CanBus, which is available on the vehicle, is responsible for communication between the engine and powertrain controllers. Many of the signals are obtained by accessing the CanBus. The signals are transferred under certain standards set by SAE [1]. Currently the J1939 [1] and its extensions like J1939-71[2] are standard for heavy duty vehicles. Older equivalents are SAE J1587 for powertrain control applications. Other sources are EBS, GPS and customized sensors installed by PATH staff. The EBS is the electronic brake control system and measures signals like wheel speed. A GPS antenna is available on the PATH truck that provides, longitude, altitude and latitude coordinates as well as the truck's cruise speed. A few sensors had been installed on the truck including accelerometers in x, y and z directions, tilt sensors,and pressure transducers for measuring brake pressure at the wheels.

The real time QNX operating system was used for data acquisition. The system was wired to the Canbus and other sensors and data was sampled at 50 Hz. A computer specialist monitored the flow of data and logged the instructions and actions by the driver and other researchers in a text file that was available to us after the test. The whole test was carried out open-loop except for some periods when cruise control was activated. Each run concentrated on gathering data required for identification of one or more components such as service brakes, compression brake, gear scheduling, etc. For successful identification we made sure that the dynamics is sufficiently rich, many times by asking the driver to pulse the commands like throttle and braking. To generate different loading scenarios, the loading of the trailer was decreased gradually from full to empty in stages during the test. At each stage the total mass of the truck was known. Abundant amount of data in distinct driving scenarios was obtained during two days of test. In the next sections we explain how the data was used for system identification and parameter estimation.

3.3.1 Measured Signals

Numerous signals are recorded during the experiments, based on different sensors, each with certain degree of accuracy, and different levels of noise. The update rates and sampling rates for the signals might also vary from one to the other based on the sensors and the port they

[1]Society of Automotive Engineers

are read from. In this section we discuss the source and accuracy of data. Then we proceed to estimate the parameters based on this measured data.

Velocity is available from J1939 as well as the EBS sensors which measure the wheel speed. GPS also provides an accurate measure of the velocity. Engine speed is known from J1939 with good accuracy. Engine torque, compression brake and transmission retarder torques are available through the J1939 port. These engine and compression torques are calculated based on static engine maps and do not reflect the very fast dynamics of the engine. However they are fast enough for our purpose. Pressure transducers are installed to measure the brake pressure at the wheels. Determining the actual force developed by service brakes will depend on a model that translates the pressure into a torque. At this stage we do not have such a model and therefore in our analysis we will dismiss portions of data in which service brakes were activated. The transmission status is available form J1939. That determines if the driveline is engaged and whether the torque convertor is locked or if a shift is in process. The driveline is always flagged engaged when not in neutral. The torque convertor was shown locked whenever the vehicle was in the third or a higher gear. Shift in process denotes the period of a gear shift when the transmission controller is in effect. The gear number could not be accessed through J1939 at the time of the test. So the J1587 port was used to get the gear numbers. Each gear ratio and the final drive ratio were available from the transmission manufacturer and were also verified using data available from J1939.

The signals recorded from the accelerometers were noisy and therefore we decided not to use these signals for obtaining accelerations. Also the signals recorded from tilt sensors had a small signal to noise ratio and therefore we could not investigate possibility of using tilt sensors for measuring the road grade. The actual road grade was extracted from the profile plans of the road.

3.3.2 Road Grade

The road tests were carried out on a part of the HOV lane of Interstate 15 north of San Diego. Within the two days of test, various driving cycles were completed in a number of round trips on a twelve kilometer stretch of highway. The test route included some overpasses with steep grades. This grade was later determined using the road plans and served as a comparison with the estimated grade. Although the GPS elevation signal was available in the test-run, the information was often noisy or corrupted as shown in the upper subplot of figure 3.1. The most accurate source for the road grade is the as-built plan available for roads and highways. Therefore we obtained the profile plans of the experimental track from Caltrans. We then carefully digitized the plans and determined the grade based on the elevations. Figure 3.1 shows the digitized elevation and grade. Note that the grade is either constant or varies linearly with distance. That is a natural result of highway design where the transition between slopes are parabolic. We used the information from GPS to determine the starting point of each test run on the digitized elevation map.

3.3.3 Determining Unknown Parameters

In the vehicle longitudinal dynamics equation 3.2, wheel radius, r_w, driveline inertia, J_e, drag coefficient, C_d, and coefficient of rolling resistance, μ, were unknown. Extra care was taken to

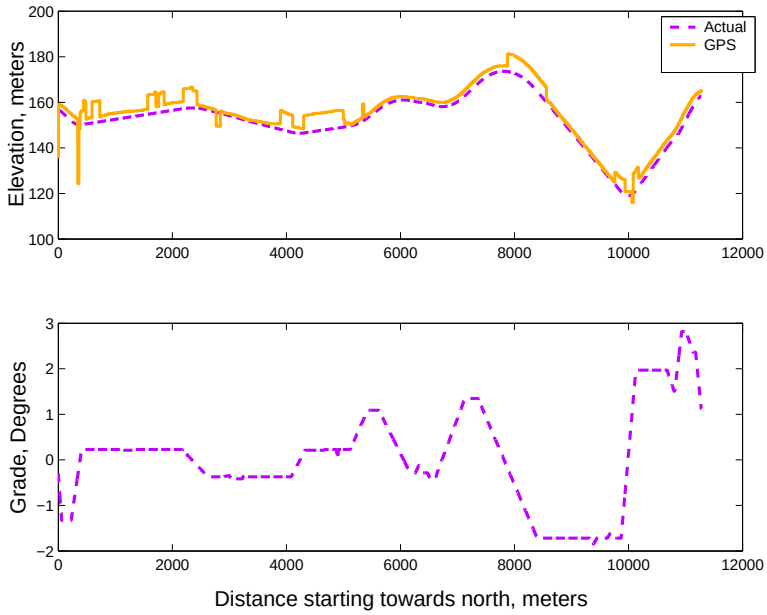

Figure 3.1: Digitized road elevation and grade.

obtain an accurate value for tire rolling radius, r_w, since other parameters are sensitive to this value. It was calculated based on the gear ratios available from the transmission manufacturer, engine speed and vehicle velocity which are available from J1939. This value was also verified by tape measurement of the drive wheel radius on site. r_g could be calculated based on this tire radius and gear ratios. J_e was not available for the experimental truck. We used a value available from another truck. However sensitivity to this parameter is not very high and deviations from this nominal value can be tolerated.

A range for values of drag coefficient and coefficient of rolling resistance for different vehicles is available in handbooks of vehicle dynamics (e.g. [42]). To select the values that fit our available data we used the vehicle longitudinal dynamics equation (4.2) and tuned the parameters of the model to make the outcomes roughly match the experimental data. The model used the engine or the retarder torque, the road grade and the selected gear that were recorded during the test and based on these inputs the accelerations were calculated. The accelerations were compared to the accelerations obtained from the test data. The drag coefficient and rolling resistance were tuned in the feasible range so that calculated and actual accelerations roughly matched each other. We found coefficient of rolling resistance of 0.006 and drag coefficient of 0.7 suitable candidates that result in good match between experiments and simulation. Figure 3.2 shows a typical test run with good match between test data and simulation results for most part of the trip. During gear changes experiments and simulation results do not have a good match. This is due to the fact that the gear shift dynamics is not considered in the longitudinal dynamics model. In the model we have assumed that velocity and engine speed are always proportionally related and that transmission is always engaged. These assumptions only result in local mismatch between model and experiments and in general the model represents the longitudinal dynamics adequately well.

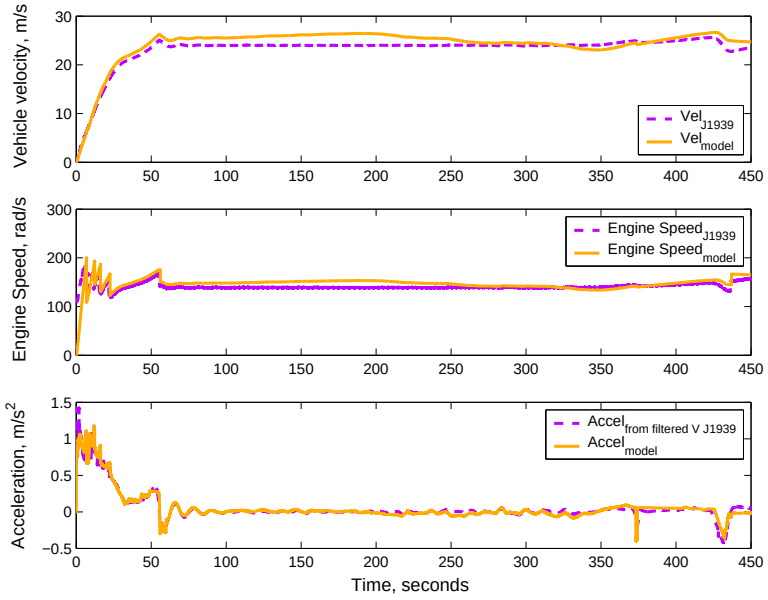

Figure 3.2: Comparison of the model and real longitudinal dynamics.

Having identified the model of vehicle longitudinal dynamics, we continue with the theory of RLS estimation and the proposed algorithm.

3.4 Recursive Least Square Estimation

In least square estimation unknown parameters of a linear model are chosen in such a way that the sum of the squares of the difference between the actually observed and the computed values, is a minimum [3]. For a linear system (e.g. model shown in (3.3)) this translates into finding the parameter(s) that minimizes the following "loss-function",

$$V(\hat{\theta}, n) = \frac{1}{2}\sum_{i=1}^{n}\left(y(i) - \phi^T(i)\hat{\theta}\right)^2 \tag{3.4}$$

Solving for the minimizing parameters we get the closed form solution as follows:

$$\hat{\theta} = \left(\sum_{i=1}^{n}\phi(i)\phi^T(i)\right)^{-1}\left(\sum_{i=1}^{n}\phi(i)y(i)\right) \tag{3.5}$$

Most of the time we are interested in real-time parameter estimation. Therefore it is computationally more efficient if we update the estimates in (3.5) recursively as new data becomes available online. The recursive form is given by:

$$\hat{\theta}(k) = \hat{\theta}(k-1) + L(k)\left(y(k) - \phi^T(k)\hat{\theta}(k-1)\right) \tag{3.6}$$

where

$$L(k) = P(k)\phi(k) = P(k-1)\phi(k)\left(1 + \phi^T(k)P(k-1)\phi(k)\right)^{-1} \tag{3.7}$$

and

$$P(k) = \left(I - L(k)\phi^T(k)\right) P(k-1) \tag{3.8}$$

$P(k)$ is normally referred to as the covariance matrix. More detailed derivation can be found in books on parameter estimation such as [3]. For convergence proof see for example the book by Johnson [18].

Eq.(3.6) updates the estimates at each step based on the error between the model output and the predicted output. The structure is similar to most recursive estimation schemes. In general most have similar parameter update structure and the only difference is the update gain $L(k)$. The scheme can be viewed as a filter that averages the data to come up with optimal estimates. Averaging is a good strategy if parameters of the model are constant in nature. However many times the parameters that we are estimating are time-varying and we are interested to keep track of the variations. In the next section the generalized RLS for time-varying parameters is discussed.

3.4.1 Recursive Least Square Estimation with Forgetting

If the values of the parameters of a system change abruptly, periodic resetting of the estimation scheme can potentially capture the new values of the parameters. However if the parameters vary continuously but slowly a different heuristic but effective approach is popular. That is the concept of forgetting in which older data is gradually discarded in favor of more recent information. In least square method, forgetting can be viewed as giving less weight to older data and more weight to recent data. The "loss-function" is then defined as follows:

$$V(\hat{\theta}, k) = \frac{1}{2}\sum_{i=1}^{k} \lambda^{k-i} \left(y(i) - \phi^T(i)\hat{\theta}(k)\right)^2 \tag{3.9}$$

where λ is called the forgetting factor and $0 < \lambda \leqslant 1$. It operates as a weight which diminishes for the more remote data. The scheme is known as least-square with exponential forgetting and θ can be calculated recursively using the same update equation (3.6) but with $L(k)$ and $P(k)$ derived as follows:

$$L(k) = P(k-1)\phi(k)\left(\lambda + \phi^T(k)P(k-1)\phi(k)\right)^{-1} \tag{3.10}$$

and

$$P(k) = \left(I - L(k)\phi^T(k)\right) P(k-1)\frac{1}{\lambda}. \tag{3.11}$$

The main difference with the classical least square method is how the covariance matrix $P(k)$ is updated. In the classical RLS the covariance vanishes to zero with time, losing its capability to keep track of changes in the parameter. In (3.11) however, the covariance matrix is divided by $\lambda < 1$ at each update. This slows down fading out of the covariance matrix. The exponential convergence of the above scheme is shown in some textbooks and research papers (See e.g. the proof provided in [7] or [18]) for the case of unknown but "constant" invariant case. In general exponential convergence in the constant case implies certain degree of tracking capability in the time varying case [9]. However rigorous mathematical analysis of tracking capabilities of an estimator when the parameters are time-varying is rare in literature and many properties are demonstrated through simulation results. Campi [9] provides rigorous mathematical arguments

that if the covariance matrix of the estimator is kept bounded the tracking error will remain bounded. Ljung and Gunnarsson present a survey of algorithms for tracking time-varying systems in [24].

The RLS with forgetting has been widely used in estimation and tracking of time-varying parameters in various fields of engineering. However when excitation of the system is poor this scheme can lead to the covariance "wind-up" problem. During poor excitations old information is continuously forgotten while there is very little new dynamic information coming in. This might lead to the exponential growth of the covariance matrix and as a result the estimator becomes extremely sensitive and therefore susceptible to numerical and computational errors [14]. This problem has been investigated by many researchers in the field and several solutions, mostly ad hoc, have been proposed to avoid covariance "wind-up". The idea of most of these schemes is to limit the growth of covariance matrix for example by introducing an upper bound. A popular scheme is proposed by Fortescue et al. [14] in which a time-varying forgetting factor is used. During low excitations, the forgetting factor is closer to unity to enhance the performance of the estimator. In another approach, Sripada and Fisher [38] propose an on/off method along with a time-varying forgetting factor for improved performance. The concept of resetting the covariance matrix during low excitations has been also investigated in [37]. Both papers provide good discussions about behavior of the system during low excitations. Kulhavy and Zarrop discuss the concept of forgetting from a more general perspective in [21].

One other popular refinement to the RLS with forgetting scheme is the concept of "directional forgetting" for reducing the possibility of the estimator windup when the incoming information is non-uniformly distributed over all parameters. The idea is that if a recursive forgetting method is being used, the information related to non-excited directions will gradually be lost. This results in unlimited growth of some of the elements of the covariance matrix and can lead to large estimation errors. Implementation of the concept of directional forgetting is again ad hoc and is reflected in updating the covariance matrix, $P(k)$. That is, if the incoming information is not uniformly distributed in the parameter space the proposed schemes perform a selective amplification of the covariance matrix. Hagglund [16] and Kulhavy [20] have developed one of the early versions of this algorithm. Bittani et al. discuss the convergence of RLS with directional forgetting in [6]. Cao and Schwartz [10] explain some of the limitations of the earlier directional forgetting scheme and propose an improved directional forgetting approach.

The estimator wind-up can also occur if we are estimating multiple parameters that each (or some) vary with a different rate. This scenario is of particular interest in the problem of mass and grade estimation where mass is constant and grade is time-varying. It will be shown by simulation later in this chapter that the single forgetting algorithm is not able to track parameters with different variation rates. Therefore it is desirable to assign different forgetting factors to different parameters. This problem is somehow similar but not equivalent to the case when excitations are non-uniform in the parameter space. Even when all the modes are uniformly excited, different rate of variations of parameters can cause trouble in estimation. An ad hoc remedy to this problem has been suggested in a few publications and is known as vector-type forgetting [35], [36] or selective forgetting [32]. The idea is again implemented in the update of covariance matrix. Instead of dividing all elements by a single λ, P is scaled by a diagonal matrix of forgetting factors:

$$P(k) = \Lambda^{-1}\left(I - L(k)\phi^T(k)\right)P(k-1)\Lambda^{-1} \tag{3.12}$$

where

$$\Lambda = diag[\lambda_1, \lambda_2, \ldots, \lambda_n]$$

in an n-parameter estimation and λ_i is the forgetting factor reflecting the rate of the change of i^{th} parameter. We found this method an effective way of keeping track of the parameters that change with different rates. The few examples of application of this scheme, to the best knowledge of the authors, can be found in [47], and [30]. Yoshitani and Hasegawa [47] have used a vector-type forgetting scheme for parameter estimation in control of strip temperature for the heating furnace. For a self-tuning cruise control Oda et al. [30] propose using vector-type forgetting for detecting step changes in the parameters of a transfer function.

Like most other modifications to RLS with forgetting, mathematical proofs for tracking capabilities of the method, to the best knowledge of the authors, do not exist. However a proof for convergence to constant parameter values can be found in [33]. In [33] a general class of RLS with forgetting is formulated and vector type forgetting is also included as a special case. Exponential convergence to constant parameter values is proven for this general class of estimators.

Before employing the vector-type forgetting, and to remedy the problems associated with different rates of variations, the authors had formulated a multiple forgetting method which has similarities to and differences from the above-mentioned schemes. It has shown very good convergence and tracking capabilities in simulation and experiments and the way it is formulated makes an intuitive sense. Since it provides some motivation on the concept of multiple forgetting, we discuss the formulation and the structure of the problem in the next section. The convergence or conditions for convergence of the algorithm remains open for future research.

3.4.2 A Recursive Least Square Scheme with Multiple Forgetting

When working on the particular mass and grade estimation problem, the authors noticed that the difficulties in RLS with single forgetting stem from the following facts: 1. In the standard method it is assumed that the parameters vary with similar rates. 2. In the formulation of the loss-function defined in (3.9) and subsequently the resulting recursive scheme, the errors due to all parameters are lumped into a single scalar term. So the algorithm has no way to realize if the error is due to one or more parameters. As a result if there is drift in a single parameter, corrections of the same order will be applied to all parameters which results in over-shoot or undershoot in the estimates. If the drift continues for sometime it might cause poor overall performance of the estimator or even the so-called estimator "wind-up" or "blow-up". It is true that we are fundamentally restricted by the fact that the number of existing equations is less than number of parameters which we are estimating, but in a tracking problem we can use our past estimation results more wisely by introducing some kind of "decomposition" in the error due to different parameters. Therefore, our intention is to conceptually "separate" the error due to each parameter and subsequently apply a suitable forgetting factor for each. Without loss of generality and for more simple demonstration, we shall assume that there are only two

parameters to estimate. We define the loss function, V:

$$V(\hat{\theta}_1(k), \hat{\theta}_2(k), k) = \frac{1}{2}\sum_{i=1}^{k} \lambda_1^{k-i} \left(y(i) - \phi_1(i)\hat{\theta}_1(k) - \phi_2(i)\theta_2(i)\right)^2 + \frac{1}{2}\sum_{i=1}^{k} \lambda_2^{k-i} \left(y(i) - \phi_1(i)\theta_1(i) - \phi_2(i)\hat{\theta}_2(k)\right)^2. \tag{3.13}$$

With this definition for the loss function the first term on the right hand side of (3.13) represents only the error of the step k due to first parameter estimate, $\hat{\theta}_1(k)$ and the second term corresponds to the second parameter estimate, $\hat{\theta}_2(k)$. Now each of these errors can be discounted by an exclusive forgetting factor. Notice that $\theta_1(k)$ and $\theta_2(k)$ are unknown. We will later replace them with their estimates, $\hat{\theta}_1(k)$ and $\hat{\theta}_2(k)$. The swapping between the estimated and the actual parameters allows us to formulate the proposed modification to the classical LS with forgetting factors.

Here λ_1 and λ_2 are forgetting factors for first and second parameters respectively. Incorporating multiple forgetting factors provides more degrees of freedom for tuning the estimator, and as a result, parameters with different rates of variation could possibly be tracked more accurately. The optimal estimates are those that minimize the loss function and are obtained as follows:

$$\frac{\partial V}{\partial \hat{\theta}_1(k)} = 0 \Rightarrow \sum_{i=1}^{k} \lambda_1^{k-i} \left(-\phi_1(i)\right) \left(y(i) - \phi_1(i)\hat{\theta}_1(k) - \phi_2(i)\theta_2(i)\right) = 0 \tag{3.14}$$

Rearranging (3.14), $\hat{\theta}_1(k)$ is found to be:

$$\hat{\theta}_1(k) = \left(\sum_{i=1}^{k} \lambda_1^{k-i}\phi_1(i)^2\right)^{-1} \left(\sum_{i=1}^{k} \lambda_1^{k-i} \left(y(i) - \phi_2(i)\theta_2(i)\right)\right) \tag{3.15}$$

Similarly $\hat{\theta}_2(k)$ will be:

$$\hat{\theta}_2(k) = \left(\sum_{i=1}^{k} \lambda_2^{k-i}\phi_2(i)^2\right)^{-1} \left(\sum_{i=1}^{k} \lambda_2^{k-i} \left(y(i) - \phi_1(i)\theta_1(i)\right)\right) \tag{3.16}$$

For real time estimation a recursive form is required. Using the analogy that is available between (3.15), (3.16) and the classical form (3.5), the recursive form can be readily deduced:

$$\hat{\theta}_1(k) = \hat{\theta}_1(k-1) + L_1(k) \left(y(k) - \phi_1(k)\hat{\theta}_1(k-1) - \phi_2(k)\theta_2(k)\right) \tag{3.17}$$

where

$$L_1(k) = P_1(k-1)\phi_1(k) \left(\lambda_1 + \phi_1^T(k)P_1(k-1)\phi_1(k)\right)^{-1}$$

$$P_1(k) = \left(I - L_1(k)\phi_1^T(k)\right) P_1(k-1)\frac{1}{\lambda_1}.$$

and similarly,

$$\hat{\theta}_2(k) = \hat{\theta}_2(k-1) + L_2(k) \left(y(k) - \phi_1(k)\theta_1(k) - \phi_2(k)\hat{\theta}_2(k-1)\right) \tag{3.18}$$

where

$$L_2(k) = P_2(k-1)\phi_2(k)\left(\lambda_2 + \phi_2^T(k)P_2(k-1)\phi_2(k)\right)^{-1}$$

$$P_2(k) = \left(I - L_2(k)\phi_2^T(k)\right)P_2(k-1)\frac{1}{\lambda_2}.$$

In the two aforementioned equations $\theta_1(k)$, $\theta_2(k)$ are unknown. We propose to replace them with their estimates, $\hat{\theta}_1(k)$ and $\hat{\theta}_2(k)$, as is customary in similar situations, such as the "separation principle" in optimal control [8]. The substitution is also justified when the actual and the estimated values are very close to each other or within the algorithm region of convergence. A convergence proof or conditions for convergence of the algorithm under this assumption, remains open for future research. Upon substitution for $\theta_1(k)$ and $\theta_2(k)$ and rearranging (3.17) and (3.18) we obtain:

$$\hat{\theta}_1(k) + L_1(k)\phi_2(k)\hat{\theta}_2(k) = \hat{\theta}_1(k-1) + L_1(k)\left(y(k) - \phi_1(k)\hat{\theta}_1(k-1)\right) \tag{3.19}$$

$$L_2(k)\phi_1(k)\hat{\theta}_1(k) + \hat{\theta}_2(k) = \hat{\theta}_2(k-1) + L_2(k)\left(y(k) - \phi_2(k)\hat{\theta}_2(k-1)\right) \tag{3.20}$$

For which the solution is,

$$\begin{bmatrix} \hat{\theta}_1(k) \\ \hat{\theta}_2(k) \end{bmatrix} = \begin{bmatrix} 1 & L_1(k)\phi_2(k) \\ L_2(k)\phi_1(k) & 1 \end{bmatrix}^{-1} \begin{bmatrix} \hat{\theta}_1(k-1) + L_1(k)\left(y(k) - \phi_1(k)\hat{\theta}_1(k-1)\right) \\ \hat{\theta}_2(k-1) + L_2(k)\left(y(k) - \phi_2(k)\hat{\theta}_2(k-1)\right) \end{bmatrix} \tag{3.21}$$

Using the fact the P_1 and P_2 are always positive it can be proved that the determinant of the matrix

$$\begin{bmatrix} 1 & L_1(k)\phi_2(k) \\ L_2(k)\phi_1(k) & 1 \end{bmatrix}$$

is always nonzero and therefore the inverse always exists. With some more mathematical manipulations, (3.21) can be written in the form of (3.6):

$$\hat{\theta}(k) = \hat{\theta}(k-1) + L_{new}(k)\left(y(k) - \phi^T(k)\hat{\theta}(k-1)\right) \tag{3.22}$$

where $L_{new}(k)$ is defined as follows:

$$L_{new}(k) = \frac{1}{1 + \frac{P_1(k-1)\phi_1(k)^2}{\lambda_1} + \frac{P_2(k-1)\phi_2(k)^2}{\lambda_2}} \begin{bmatrix} \frac{P_1(k-1)\phi_1(k)}{\lambda_1} \\ \frac{P_2(k-1)\phi_2(k)}{\lambda_2} \end{bmatrix} \tag{3.23}$$

The proposed method incorporates different forgetting factors for each parameter. To this end, it does what the vector-type forgetting method does. Eq. (3.22) is similar in form to the standard update of (3.6). However the gains of the standard and the proposed form are different. Specifically the former has a crossterm $P_{12}(k-1)$, while the latter does not. In other words the covariance matrix of the proposed method is diagonal. This will result in update of the two parameters proportional to $P_1(k)$ and $P_2(k)$.

In short, introduction of the loss-function (3.13) with decomposed errors and different forgetting factors for each have two distinct implications:

1) Parameters are updated with different forgetting factors. That is done by scaling the covariances by different forgettings. This is more or less what is done in the RLS with vector-type forgetting as well. However this approach is based on minimization of a loss-function.

2) It decouples the updating step of the covariance of different parameters. This is different from standard RLS or RLS with vector-type forgetting. It is more similar to the "simplified" algorithms mentioned in second chapter of [3]. The authors believe that when the parameters are independent of each other this makes an intuitive sense.

This scheme did well in both simulation and experiments of mass-grade estimation. The performance is very similar to the RLS with vector forgetting when similar forgetting factors are used. However we observed in some simulations that if the value of the forgetting factors are picked in a way that mismatches real rate of variations of the parameters, RLS with vector forgetting sometimes winds up. In such a situation the estimator was excessively sensitive to noise. On the other hand, the proposed scheme behaved well in this scenario and mismatch between forgetting and true rate of variations did not cause the windup behavior. In other words the proposed algorithm seems to be "forgiving" to the choice of forgetting factors. In the following section we carefully select the forgetting factors of the vector-type forgetting RLS so that the response compares favorably with the decoupled multiple forgetting that we proposed.

3.4.3 Comparison of Single and Multiple Forgetting Methods

We first use simulated data to test a recursive scheme for estimation of mass and grade. The simulated data was generated using the vehicle dynamics model given in (3.2) and by assuming different road grade profiles and feasible mass and parameters for a heavy duty vehicle. A feasible fuelling pattern was chosen. Variation of fuelling is important in exciting all modes of the system and consequently allows better estimation results. Therefore in generating the fuelling command this was taken into account. The engine torque was then calculated based on fuelling rate and engine speed by using the engine torque map. At this stage we assumed that no gear change occurs during the estimation process. In the next sections, we will discuss the issue of gear change and explain how it can be incorporated in experimental estimation. We use a recursive least square scheme for estimating and tracking the parameters. For initialization, we employ a direct least square on a batch of first few seconds of data. This initializes the estimates and the P matrix. Sampling rate of all signals is 50 Hz.

First we used the RLS with single forgetting for estimation of mass and grade. For the reasons explained in previous sections of this chapter the results were not promising at all. First we considered a constant mass and step changes in grade. The data that we used was clean from any noise. Figure 3.3 shows the estimation results. We observe big overshoots or undershoots in both mass and grade estimates during step changes in grade or fuelling. Nevertheless we see a relatively fast convergence back to the real parameter values after the deviations. That is in line with the proofs of convergence of RLS with or without forgetting to constant parameter values. The spikes during the steady-state are due to step changes in fuelling rate which act similar to a disturbance to the system. To this end, despite the local misbehavior we can still get some estimates for both parameters. The main difficulty of the approach appears when one of the parameters, here the grade, starts varying continuously (as opposed to staying piecewise constant). The algorithm shows very poor tracking performance in such a scenario.

Figure 3.4 shows the estimator performance when grade variations are sinusoidal. The well-

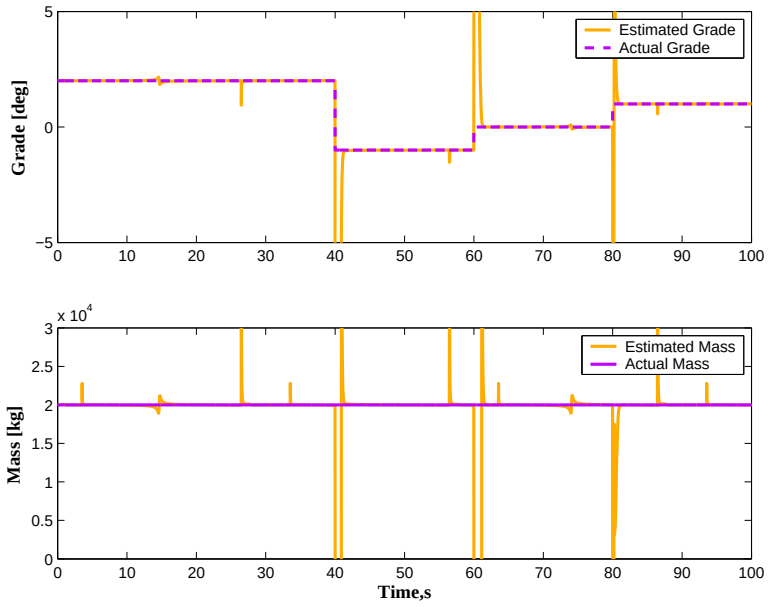

Figure 3.3: Estimation of mass and grade using RLS with a single forgetting factor of 0.8 when grade is piecewise constant. Sampling rate is 50 Hz. The spikes during steady-state are due to step changes in fuelling rate.

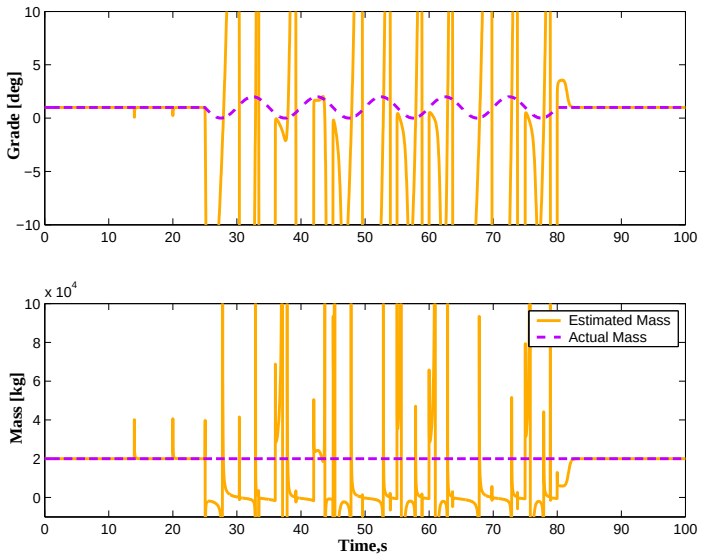

Figure 3.4: Estimation of mass and grade using RLS with a single forgetting factor of 0.9 when grade variations are sinusoidal. Smaller forgetting factors for grade resulted in worsens the performance. The spikes during steady-state are due to step changes in fuelling rate.

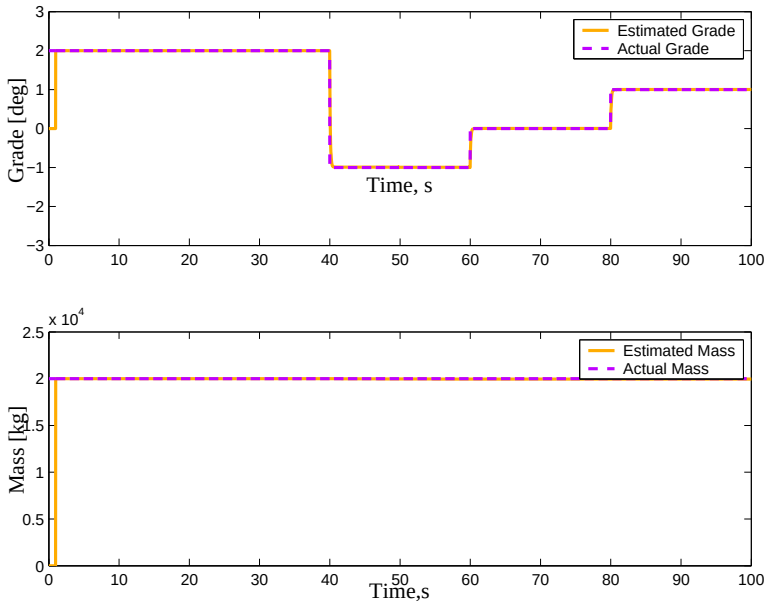

Figure 3.5: Estimation of mass and grade using RLS with multiple forgetting factors of 0.8 and 1 respectively for grade and mass.

known phenomenon of estimator "blow-up" or "wind-up" can be seen during grade changes and errors in both mass and grade estimates become very large. The estimates converge back to the real values only when the grade becomes constant. Here a forgetting factor of 0.9 is chosen. We noticed that reducing the forgetting factor will only worsen the problem. When noise is introduced in the data, the performance is sacrificed even more. Increasing the forgetting factor to 1 (classical RLS) will eliminate the big overshoots, but will average all the past data equally. This can result in meaningless estimates for both parameters. As explained in the formulation of the problem, the reason for the poor performance of RLS with single forgetting is that when an error is detected the estimates for both parameters are updated without differentiating between the ones that vary faster and those that do not vary as often or are constant. This causes overshoot/undershoot in the estimates. If one parameter continues drifting, the estimation errors add up to result in what was seen in the previous figures.

We carried out simulations using RLS with multiple forgetting factors and showed that this scheme can resolve the problems encountered with single forgetting. Figure 3.5 shows the performance of the estimator when grade goes through step-changes. In this example forgetting factors of 0.8 and 1.0 are chosen for grade and mass respectively. Unlike estimation with single forgetting, the estimation is very smooth and the estimates converge much faster during step changes. Also the spikes due to step change in fuelling rate disappear. Because a forgetting factor of 1.0 is chosen for mass, the mass estimates are not as sensitive to changes in grade.

We also tried sinusoidal variations in grade. The results are shown in Figure 3.4.3. The grade is tracked very well and with very small lag. The rate of change shown for the grade is much faster than the norm on the roads. Even with a much higher speed of variations, the estimator does not ill-behave. In simulation we observed that if the forgetting factors are chosen so that they roughly reflect relative rate of change of parameters, parameter changes are tracked

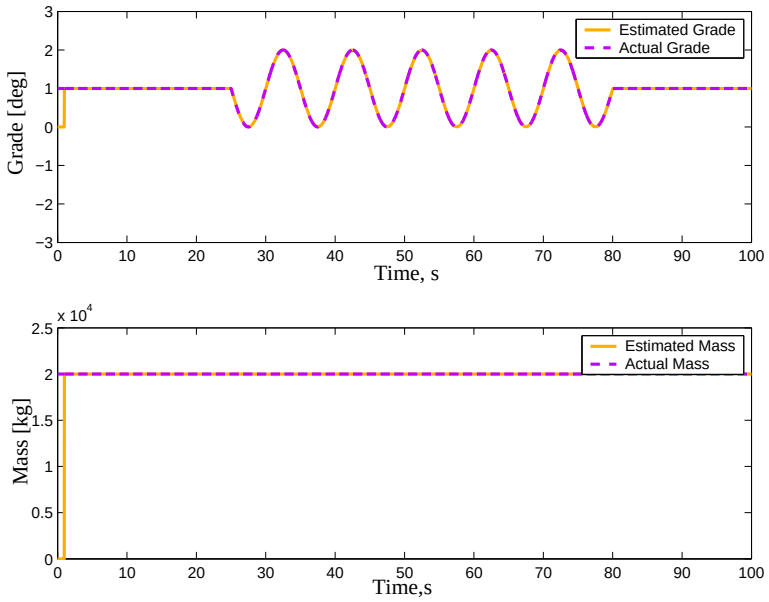

Figure 3.6: Estimation of mass and grade using RLS with multiple forgetting factors of 0.8 and 1 respectively for grade and mass.

well.

A summary of some other scenarios is shown in Table 3.1. The results shown in this table are based on numerical data that is not noisy. Simulations with data contaminated by noise show that noise deteriorates the performance of the single forgetting estimation. The multiple forgetting scheme showed much better robustness in presence of noise.

3.5 Performance of the Estimator with Experimental Data

In the previous sections of this chapter, the estimation problem was formulated, a solution was proposed and it was shown in simulations that it performs well in estimating mass and keeping track of time-varying grade. The demonstration was either in a noise-free environment or when white noise was added to the signals. In a real scenario the situation can become more challenging due to higher level of uncertainties. The signals are potentially delayed and many times the signals are noisy and biased in one direction rather than being only affected by pure white noise. Moreover, the delay or noise level in one signal is normally different from the other signals. Finally, note that what is available from sources like J1939 is normally not the true value of an entity but an estimate of the true value through the vehicle/engine management system. Unmodelled dynamics of the system might result in poor estimation.

The signals in a natural experimental cycle may not always be persistently exciting. As discussed before lack of good excitation results in poor estimates or even cause estimator windup. In our case, if the acceleration is constant and there is no gear change, we are not able to

Scenario	Single Forgetting	Multiple Forgetting
Constant grade Constant mass	good estimation	good estimation
Step changes in grade Constant mass	some overshoots in estimates	good estimation
Linear change of grade Constant mass	bad estimation	good estimation
Sinusoidal change of grade constant mass	bad estimation	good estimation
Sinusoidal change of grade Linear variations of mass	bad estimation	estimates with some lag

Table 3.1: Comparison of the performance of single and multiple forgetting RLS algorithms

observe enough to determine both mass and grade. In this case the longitudinal dynamics equation represents essentially a single mode, making it literally impossible to estimate the two unknowns. Therefore it is important that in online estimation, rich pieces of data are detected and used for estimation of both parameters. Once a good estimate for mass which is constant is obtained tracking of variations of grade would be possible even during low or constant levels of acceleration.

3.5.1 Modification for Reducing Signal Noise Effect

Direct implementation of (3.2) in least square estimation requires differentiation of velocity and engine speed signals. In a noisy environment, differentiation is not very appealing. It will magnify the noise levels to much higher values and the differentiated data may not be useable. In order to circumvent this problem we will first integrate both sides of (3.2) over time and apply the estimation scheme to the new formulation. Assuming that mass and coefficient of rolling resistance are constant, integration of both sides yields:

$$v(t_k)-v(t_0)=\frac{1}{M}\int_{t_0}^{t_k}(\frac{T_e(t)-J_e\dot{\omega}(t)}{r_g(t)}-F_{fb}(t)-F_{aero}(t))dt-\frac{g}{\cos(\beta_\mu)}\int_{t_0}^{t_k}\sin(\beta+\beta_\mu)dt \quad (3.24)$$

We can rewrite the above equation in the form of (3.3),

$$y=\phi^T\theta,\ \phi=[\phi_1,\phi_2]^T,\ \theta=[\theta_1,\theta_2]^T$$

where this time

$$y(k)=v(t_k)-v(t_0)$$

$$\theta=[\theta_1,\theta_2]^T=[\frac{1}{M},\ \frac{\int_{t_0}^{t_k}\sin(\beta+\beta_\mu)dt}{(t_k-t_0)}]^T$$

and

$$\phi_1=\int_{t_0}^{t_k}(\frac{T_e-J_e\dot{\omega}}{r_g}-F_{fb}-F_{aero})dt,\ \phi_2=-\frac{(t_k-t_0)g}{\cos(\beta_\mu)}$$

Notice that ϕ_2 is multiplied by $(t_k - t_0)$ and θ_2 is divided by it. This is to keep the unknown parameter θ_2 away from growing fast with time. In this fashion if the grade, β, is constant, θ_2 will remain constant as well. Employing integration instead of differentiation helped avoid some serious issues related to signal noise.

3.5.2 Estimation in Normal Cruise: No Gearshift

We first evaluate the estimation scheme with experimental data when the gear is constant. Similar to the approach in simulations we use a batch in the first few seconds of estimation to initialize the estimation scheme. Good initial estimates are obtained only when the chosen batch is rich in excitations. Better estimates can be obtained with a smaller batch when the acceleration has some kind of variation during the batch. The RLS with multiple forgetting was used during the rest of the travel for estimation and tracking.

To reduce the high frequency noise, the torque and velocity signals were passed through a second order butterworth filter before they were used in the estimation. The sampling frequency is 50 Hz, and therefore the Nyquist frequency is 25 Hz. We use the cutoff frequency of 25 Hz for the filter, to ensure that aliasing will not occur. Figure 3.7 shows the estimation results for

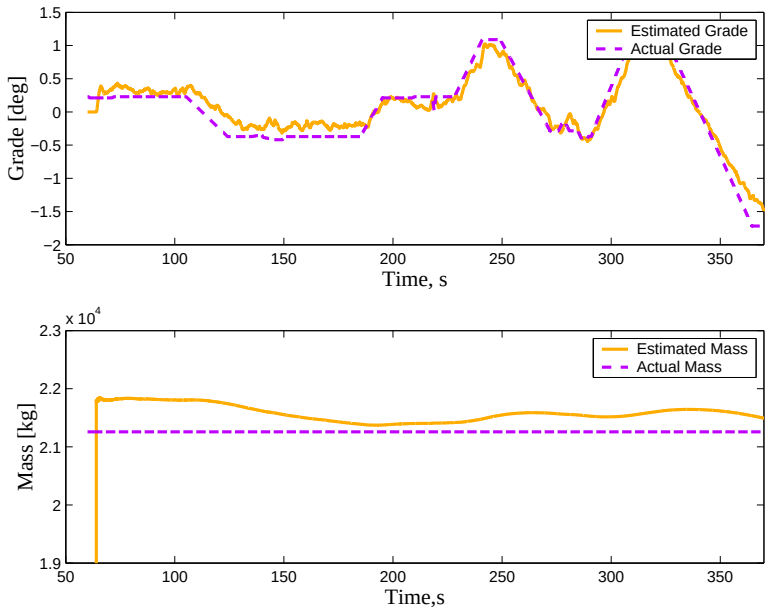

Figure 3.7: Estimator's performance during normal cruise when the gear is constant. Forgetting factors for mass and grade are 0.95 and 0.4 respectively. RMS error in mass is 350 kg and RMS grade error is 0.2 degrees.

more than five minutes of continuous estimation. The gear was constant throughout this period. The initial four seconds of data was processed in a batch to generate the initial estimates. For the recursive part forgetting factors of 0.95 and 0.4 were chosen for mass and grade respectively. While mass is constant, a slight forgetting acts as a damping effect on the older information and makes the mass estimate a little more responsive to new information. This showed to result in

further convergence of mass to its true value. In this estimation the root mean square (RMS) error in mass is 350 kg and the maximum error is 2.8%. During the recursive section the error in mass reduces down to a maximum of 1.7%. The RMS error in grade is 0.2 degrees. It can be seen that grade is estimated well during its variations.

Next we will remedy the estimation problem when gear changes occur.

3.5.3 Estimation Results During Gearshift

In the longitudinal dynamics Eq. (4.2) we assume that engine power passes continuously through the driveline to the wheels. This assumption is valid only when the transmission and torque convertor are fully engaged. During a gear change, transmission disengages to shift to the next gear and during this time the flow of power to the wheels is reduced and in the interval of complete disengagement no torque is passed over to the wheels. Moreover the assumption that vehicle speed is proportional to the engine speed by some driveline ratio is not in effect during this transition and the engine speed goes through abrupt changes while the change in vehicle velocity is much smoother. Therefore relying on (4.2) for estimation will result in very big

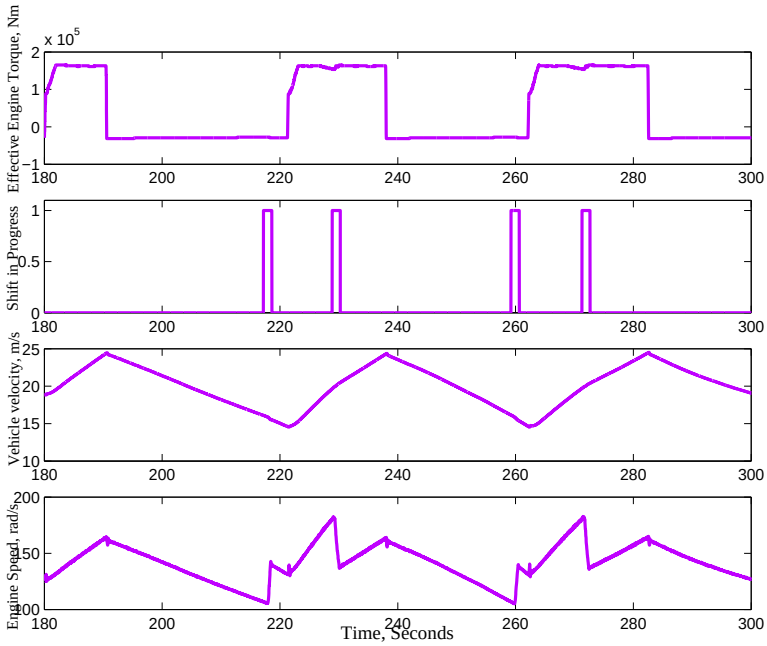

Figure 3.8: The response during a cycle of pulsing the throttle

deviations during gearshift. The bigger the deviations are the longer it takes the estimator to converge back to the true parameter values.

Modelling the dynamics during a shift is not simple due to natural discontinuities in the dynamics. Besides the period when the transmission is in control does not take more than two seconds and therefore it is not really necessary to estimate the parameters during this short period. Therefore we decided to turn off the estimator at the onset of a gearshift and turn it back on a second or two after the shift is completed. The estimates during the shift are set

equal to the latest available estimates. Also the new estimator gain is set equal to the latest calculated gain. This approach proved to be an effective way of suppressing unwanted estimator overshoots during gear shift. Figure 3.8 shows the engine torque, shift status, vehicle velocity

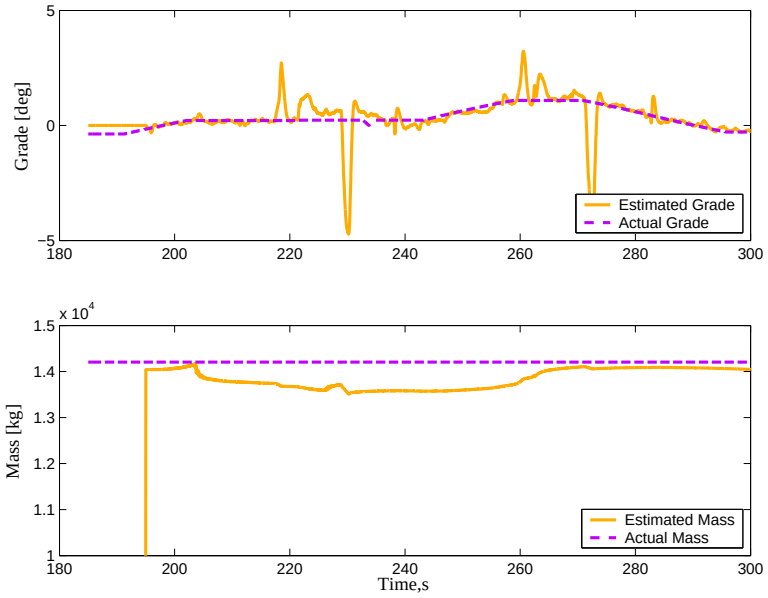

Figure 3.9: Estimator's performance when it is always on. Forgetting factors for mass and grade are 0.95 and 0.4 respectively. The RMS errors in mass and grade are 420 kg and 0.77 degrees respectively.

and engine speed during part of an experiment. We had asked the driver to pulse the throttle off and on and therefore as seen in the torque plot, the torque is either at its maximum or drops down to zero. Also two gear shifts occur during this time window. As mentioned before the variations in velocity are smooth but the engine speed has jump discontinuities both during gear shift and during the throttle on/off. Upon using the estimator with no on/off logic we observed big overshoots in the estimates during both the gearshift and the throttle on/off. The results are shown in Figure 3.9. The root mean square error in mass is 420 Kilograms and the RMS grade error is 0.77 degrees which is a large error. We then used the estimator with the on/off logic. The results are shown in figure 3.10. The estimation has improved considerably due to the estimator deactivation during the shifts. The deviations due to throttle pulsation exist as before but the magnitude of these deviations are small and they fade away quickly. In this estimation the root means square error in mass is 310 kilograms and the RMS grade error is 0.24 degrees which are quite improved due to the employed estimator logic.

3.5.4 Sensitivity Analysis

Earlier in this chapter the coefficient of rolling resistance and the drag coefficient were calculated based on matching the model outcomes and experimental results. We mentioned that these estimates are rough estimates that meet our needs. We are in general interested to know how

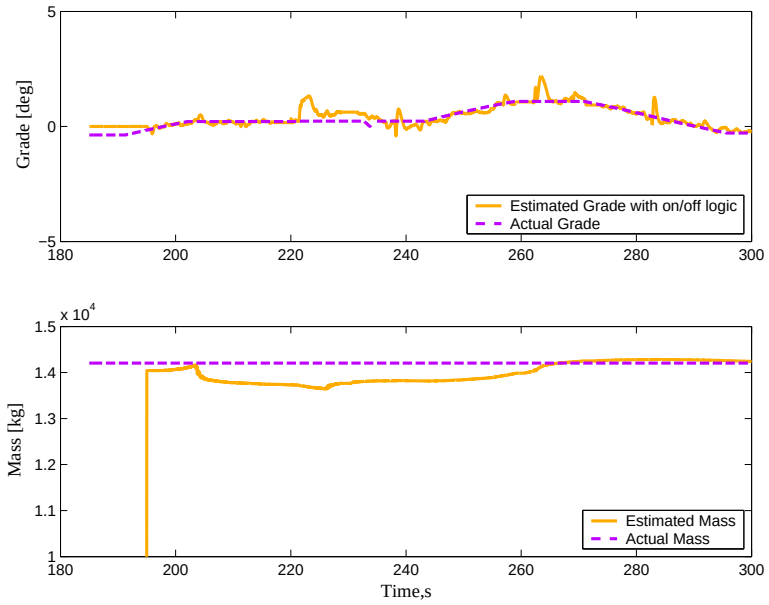

Figure 3.10: Estimator's performance when it is turned off during shift. Forgetting factors for mass and grade are 0.95 and 0.4 respectively. The RMS errors in mass and grade are 310 kg and 0.24 degrees respectively.

much the mass and grade estimation results are sensitive to these parameters. In other words we want to analyze the sensitivity of the estimation scheme with respect to these parameters.

For this analysis we vary the rolling resistance and drag coefficient one at a time and observe the performance of the estimates and based on these results provide a sense on the sensitivity of the system. We perform the analysis with the experimental set of data used in section 3.5.2 of this chapter. Figure 3.11 shows the sensitivity of the estimates with respect to drag coefficient and rolling resistance. Variations in the coefficient of rolling resistance only affect the grade estimate. That is because the rolling resistance and grade affect the longitudinal dynamics in the same way. In a realistic range, a 50% variation of the coefficient of rolling resistance caused, in the worst case, less than 25% change in the RMS error of grade estimates. The drag coefficient selection influenced both mass and grade estimates. Here 25% change in drag coefficient within a feasible range, cause less than 25% change of error in grade and mass estimates.

In the analysis of this chapter the wheel radius was known accurately. However to see how would an incorrect measure of wheel radius affect the estimation results, we carried out sensitivity analysis for different wheel radii. The results are shown in Figure 3.12. The results show that grade estimates are not very sensitive to errors in wheel radius while sensitivity is roughly 1 for mass estimate. This was expected as wheel radius directly affects the available traction torque for acceleration which in turn directly affects mass estimates. Therefore it is important that accurate value for wheel radius is used to successfully estimate the mass.

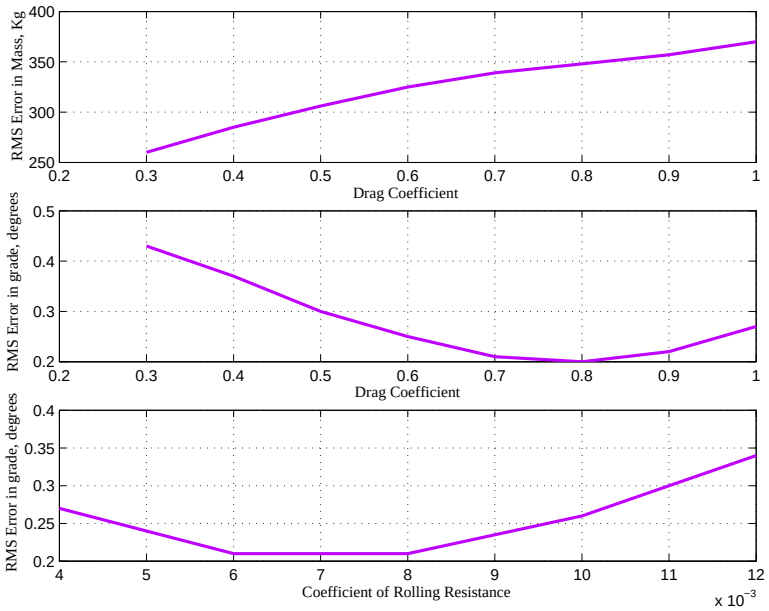

Figure 3.11: Sensitivity of the estimates with respect to drag coefficient and rolling resistance. Forgetting factors for mass and grade are 0.95 and 0.4 respectively. Nominal mass is 21250 kg.

3.6 Conclusions

Simultaneous estimation of vehicle's mass and road grade is a challenging problem. Previous work concentrated on either estimating only one or assumed existence of additional sensors on the vehicle which could be used to estimate one of the unknowns. In this chapter a recursive least square scheme with forgetting is proposed for simultaneous online estimation of mass and grade. We show in simulations that a single forgetting factor could not estimate parameters with different rates of variation. Ways to incorporate more than one forgetting factor for estimation of multiple parameters with different rates of variation are discussed and the effectiveness of the algorithm with multiple forgetting in estimating a constant mass and time-varying grade is shown with simulations.

Results of estimation of mass and grade with experimental data are then shown. The data was obtained from experiments that were carried out on Interstate 15 in San Diego in the August of 2002 with an experimental heavy duty vehicle. The experiment setup, the measured signals and their source and issues like sampling rate and accuracy are briefly discussed. Using this data we first verify that the vehicle model captures the longitudinal dynamics accurately for most part of travel. The RLS with multiple forgetting which was successful in simulations was tested and proved effective with the experimental data. The real life issues like lack of persistent excitations in certain parts of the run or difficulties of parameter tracking during gear shift are explained and suggestions to bypass these problems are made. Without gear shift and in the presence of persistent excitations mass and grade are estimated with good precision and variations of grade are tracked. When gearshifts takes place, the estimator shows large overshoots and it takes a

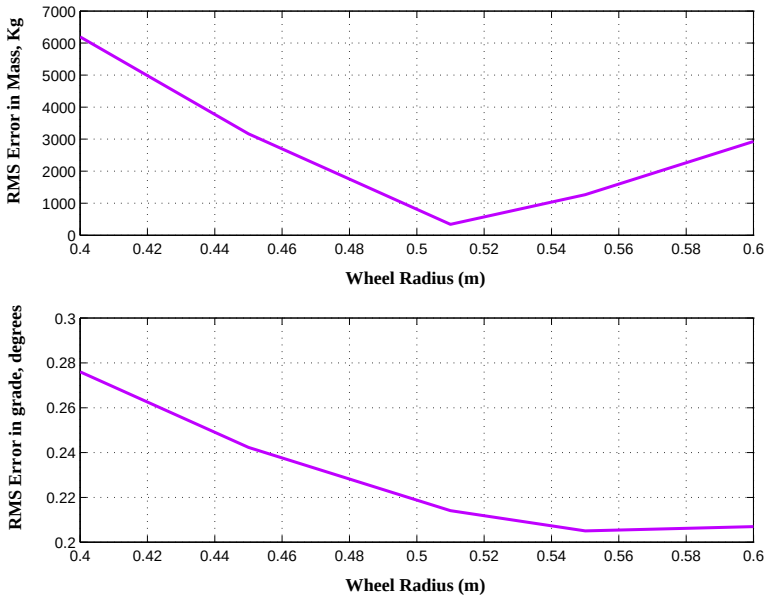

Figure 3.12: Sensitivity of the estimates with respect to wheel radius. Forgetting factors for mass and grade are 0.95 and 0.4 respectively. Nominal mass is 21250 kg.

few seconds for these deviations to damp out. We proposed turning off the estimator during and shortly after a gearshift. The estimation results are improved by this provision. Sensitivity analysis demonstrates that estimation is not overly sensitive to uncertain parameters of the system including drag coefficient and rolling resistance.

In its present form, the proposed scheme can be employed in a real-time application with caution, since its convergence and region of convergence has not been shown. Care should be exercised in choosing the batch initialization procedure and in ensuring persistent excitation. There is room for including some more logical checks and routines that can make the algorithm more robust to a variety of operating situations. Inclusion of a logic to detect areas of high or low excitations is one example which can save the estimator from a potential windup. With the added robustness the proposed scheme can be used alone or along with other sensor or model based schemes for online estimation. We are planning to test this scheme in conjunction with the longitudinal control module and analyze potential improvements to the heavy duty vehicle automation.

Chapter 4

Adaptive and Optimal Braking Control under Actuator Constraints

4.1 Introduction

Compression braking is a standard mechanism on today's heavy vehicles and is a suitable actuator in speed control applications. For example, in Eaton-Vorad collision-warning system with SmartCruise EVT-V300, compression braking is automatically activated when a collision is imminent [13]. In the existing compression braking systems, the retarding power level is quantized and depends on the engine speed and a selected number of cylinders activated by the driver. For example two, four or six cylinders can be activated to generate three levels of retarding power for a certain engine speed [25]. While successful implementation of the discrete compression brake mechanism in automated longitudinal control has been demonstrated in experiments [13], more flexibility is expected with the more advanced continuously variable compression braking systems. A continuous spectrum of retarding powers can be achieved in a camless engine and by variable valve timing. A detailed crank angle based model of such a continuous compression brake system is developed in [27] and validated with experimental data from a dynamometer. In [11] a nonlinear control design has been proposed which uses a continuously variable compression braking system in longitudinal control applications. To deal with large parameter uncertainties particular to heavy vehicles, a model reference adaptive algorithm is proposed in [12] which uses a continuous compression braking system.

The experiment results on coordinated use of compression and service brakes for speed control are given in [13]. In this paper, Druzhinina et al. successfully used a PID control technique to determine the desired retarding torque and use simple logic to split this torque between a discrete compression braking system and friction brake. The controller decided the number of cylinders to be activated for compression braking. Torque deficit was compensated by use of service brakes.

If continuous compression braking system is used instead, range of possibilities for control increases as then the brake valve timing can be chosen in a continuous range in addition to the service brake command. Even in the continuously variable compression brakes, there are limits on the brake valve timing and its rate of change. Incorporating these considerations is not possible by a simple logic-based PID control. Constrained optimization is necessary to make

the best use of compression brakes and service brakes given their saturation limits. This goal can be achieved by a model predictive control design.

In this chapter, we design an adaptive model predictive controller for coordination of continuously variable compression brakes and service brakes. MPC takes the actuator constraints into account, when calculating the control command. Moreover addition of a parameter estimation scheme, improves the robustness of the controller to uncertainties in vehicle mass. Estimation of the road grade disturbance enhances the performance further, by contributing to feedforward control. The proposed methodology can be used in automated longitudinal control applications such as platooning and adaptive cruise control. Also in manual driving, the brake-by-wire system can use both retarding mechanisms to achieve the requested deceleration. In the next section we summarize the longitudinal dynamics model of the vehicles and the braking systems. Then an adaptive model predictive control methodology is briefly explained. Simulation results are accompanied by analysis on performance of the controller in presence of control design constraints and parameter uncertainties.

4.2 Longitudinal Dynamics Model

Assuming that there is no wheel slip, which is a good assumption at highway cruise speeds, the longitudinal dynamics equation of the vehicle can be written as follows:

$$M\dot{v} = \frac{-T_{cb} - J_e\dot{\omega}}{r_g} - \frac{T_{fb}}{r_w} - F_{aero} - F_{grade} \tag{4.1}$$

In this equation, M is the total mass of the vehicle, v is the velocity and ω is rotational engine speed, T_{fb} is total friction braking torque at the wheels and T_{cb} is the compression braking torque at the flywheel. The assumption is that transmission and the torque converter are fully engaged and the torque is passed to the wheels without any loss. This is a good assumption when the truck is running at a constant gear, which is the case if the operating conditions do not vary much. J_e is the powertrain inertia. r_g is the wheel radius divided by total gear ratio:

$$r_g = \frac{r_w}{g_d g_f}$$

where r_w is the wheel radius, g_d is the gear ratio and g_f is the final drive ratio. The aerodynamic resistance is given by

$$F_{aero} = \frac{1}{2} C_d \rho A v^2$$

where C_d is the drag coefficient, ρ is air density and A is frontal area of the vehicle. The combined force due to road grade (β) and the rolling resistance of the road (μ) is given by

$$F_{grade} = Mg(\mu \cos\beta + \sin\beta),$$

where g is the gravity constant. Here $\beta = 0$ corresponds to no inclination, $\beta > 0$ corresponds to uphill grade and $\beta < 0$ represents downhill.

For linear control designs, equation (4.1) can be linearized around a nominal operating velocity v^o:

$$M\delta\dot{v} = \frac{-\delta T_{cb} - J_e\delta\dot{\omega}}{r_g} - \frac{\delta T_{sb}}{r_w} - C_d\rho A v^o \delta v - \delta F_{grade} \tag{4.2}$$

The operator, δ, represents deviation of each variable from the equilibrium values. Choosing a sampling time of T_s, the above equation can be discretized as follows:

$$\begin{aligned}&\delta v(k+1) = \\ &\left(1 - \frac{2T_s K_{aero} v^o}{M_{eff}}\right) \delta v(k) \quad + \frac{T_s}{M_{eff}} \left(-\frac{\delta T_{cb}(k)}{r_g} - \frac{\delta T_{sb}(k)}{r_w} - \delta F_{grade}(k)\right)\end{aligned} \tag{4.3}$$

where

$$K_{aero} = \frac{1}{2} C_d \rho A \quad M_{eff} = M + \frac{J_e}{r_g}$$

and J_e is the driveline inertia. For the control purpose, velocity of the vehicle, v, engine speed, ω, compression braking torque, T_{cb} and gear number, g_d, can be obtained from vehicle's CAN[1]. The service brake torque is normally hard to measure but can be estimated based on the brake model presented later in this chapter. The mass is either known or is estimated using an estimation scheme. Other vehicle parameters like wheel radius and gear ratios are fixed values which are normally known in advance. In general road grade is unknown and therefore acts as an unmeasured disturbance to the system. However it can be determined using an online estimation scheme or using GPS coordinates combined with a digital map of the road. Next we will explain the dynamic models of compression brake and service brakes used in this study.

4.2.1 Compression Brake Model

In [27] a detailed crank angle based model for a continuously variable compression brake is developed and validated with experimental data. The model takes into account the transient interactions between individual cylinder intake and exhaust gas process, turbocharger dynamics and vehicle dynamics. The detailed model is capable of simulating transitions from combustion to braking by cutting-off the fuel injection and initiating the brake event. For control design purposes, identification methods are used to reduce this detailed model to a set of low order models for different operating conditions [28]. In this reduced form the engine braking torque at steady-state can be specified as a nonlinear function of engine speed and brake valve opening as follows:

$$T_{cb}^{st}(\omega, BVO) = \alpha_0 + \alpha_1 \omega + \alpha_2 BVO + \alpha_3 \omega BVO \tag{4.4}$$

where T_{cb}^{st} is the steady-state compression braking torque and BVO is the brake valve opening in crank angle degrees. The operating range for brake valve opening is between 620 and 680 degrees. When T_{cb} is in Newton-meter, BVO is in degrees and ω is in rad/sec, the parameters of the model are:

$$\alpha_0 = -1893 \quad \alpha_1 = 48.13 \quad \alpha_2 = 2.8588 \quad \alpha_3 = -0.07839$$

In this work, the nominal downhill grade is chosen to be $\beta^o = -1.25$ degrees. At equilibrium, we assume that the truck is in fourth gear, cruising at $v^o = 20 m/s$. Using the parameters of a PATH experimental truck, the total driveline ratio, ${r^o}_g$, for the fourth gear is 0.1102. Therefore the operating engine speed is:

$$\omega^o = \frac{v^o}{r_g^o} = 181.47 \frac{rad}{s} \approx 1800 rpm$$

[1]Control Area Network

Our assumption is that this constant speed is maintained by application of compression brakes only and service brakes are not applied at this equilibrium point. The corresponding (nominal) brake valve timing, BVO, can be calculated from equation (4.4) to be $BVO^o = 650$ degrees. We define the compression brake control command, u_{cb}, to be the deviation from this nominal value: $u_{cb} = BVO - BVO^o$. The linearized model for steady-state engine brake torque is then:

$$\delta T_{cb}^{st} = 2.82\delta\omega + 11.36u_{cb} \tag{4.5}$$

Given that brake valve opening, BVO, is limited between 620 and 680 degrees, upper and lower hard constraints imposed on u_cb are:

$$-30 \leq u_{cb} \leq 30$$

For control design purpose, the dynamics of the compression braking event can be modelled by a first order lag:

$$\delta\dot{T}_{cb}(t) = -\frac{1}{\tau_{cb}}(\delta T_{cb}(t) - \delta T_{cb}^{st}(t)) \tag{4.6}$$

where τ_{cb} is the compression brake time constant. Using Euler approximation for the derivative term, the discrete form of the model is written as:

$$\delta T_{cb}(k+1) = (1 - \frac{\delta T_s}{\tau_{cb}})T_{cb}(k) + \frac{\delta T_s}{\tau_{cb}}\delta T_{cb}^{st} \tag{4.7}$$

The time constant of the compression braking event is much smaller than time constant of the vehicle velocity dynamics. Therefore we do not expect to see large sensitivity to this time constant.

4.2.2 Service Brake Model

There are various nonlinearities like dead zones, different brake activation and release dynamics and delays which complicates an accurate model of a friction brake [25]. Yet a fair model can be obtained by using a linear static model and a first order lag which represents the dynamics. Since we are using the service brakes moderately and only to compensate for torque deficits in this work, uncertainties due to brake overheating and saturations will not be a big issue.

The static braking torque at the wheel is proportional to the air pressure at the wheels as follows:

$$T_{sb}^{st} = \mu_d r_d A_d P_d \tag{4.8}$$

where μ_d is the friction coefficient between the brake drum and brake pad. r_d is the brake drum radius and A_d is area of diaphragm. P_s is applied brake pressure on the diaphragm. This pressure is related to the command voltage, u_{sb}, by a constant, κ_s, determined by the manufacturer:

$$P_s = \kappa_s u_{sb}$$

The values were experimentally identified for one of the PATH experimental trucks by PATH researchers. The lumped coefficient from the command voltage to total braking torque was determined to be $272.5\frac{Nm}{volt}$. Given that the nominal service brake torque, T_{sb}^o, is zero, we can write:

$$\delta T_{sb}^{st} = 272.5u_{sb} \tag{4.9}$$

The range for command voltage of the experimental truck was zero to ten volts. However it was determined that at five volts the wheels would lockup. Therefore we constrain the command voltage between zero and five volts:

$$0 \leq u_{sb} \leq 5$$

We assume that the braking toque is available at four wheels. The dynamics of the brake is modelled by a first order lag:

$$\delta \dot{T}_{sb}(t) = -\frac{1}{\tau_{sb}}(\delta T_{sb}(t) - \delta T_{sb}^{st}(t)) \tag{4.10}$$

where τ_{sb} is the service brake time constant. The discrete form is:

$$\delta T_{sb}(k+1) = (1 - \frac{T_s}{\tau_{sb}})\delta T_{sb}(k) + \frac{T_s}{\tau_{sb}}\delta T_{sb}^{st} \tag{4.11}$$

Coordination of the service brakes with compression brakes is based on a model predictive control design which is explained next.

4.3 Model Predictive Control Design

A brief summary of the specific MPC design, used in this work is provided in this section. For more details see [22, 26].

We define the state vector, $x = \begin{bmatrix} \delta v(k) & \delta T_{cb}(k) & \delta T_{sb}(k) \end{bmatrix}^T$ and augment equations (4.3), (4.7) and (4.11) to get:

$$\begin{aligned} x(k+1) &= Ax(k) + B_u u(k) + B_w w(k) \\ y(k) &= Cx(k) \end{aligned} \tag{4.12}$$

where the control inputs are compression brake and service brake commands:

$$u(k) = \begin{bmatrix} u_{cb}(k) & u_{sb}(k) \end{bmatrix}^T$$

and the disturbance is

$$w(k) = -Mg\left((\mu\cos\beta + \sin\beta) - (\mu\cos\beta^0 + \sin\beta^0)\right)$$

The system matrices are:

$$A = \begin{bmatrix} 1 - \frac{2T_s K_{aero} v^o}{M_{eff}} & -\frac{T_s}{r_g M_{eff}} & -\frac{T_s}{r_w M_{eff}} \\ \frac{2.82T_s}{r_g \tau_{cb}} & 1 - \frac{T_s}{\tau_{cb}} & 0 \\ 0 & 0 & 1 - \frac{T_s}{\tau_{sb}} \end{bmatrix}$$

$$B_u = \begin{bmatrix} 0 & 0 \\ 11.36\frac{T_s}{\tau_{cb}} & 0 \\ 0 & 272.5\frac{T_s}{\tau_{sb}} \end{bmatrix} \quad B_w = \begin{bmatrix} \frac{T_s}{M_{eff}} \\ 0 \\ 0 \end{bmatrix}.$$

We want to regulate the velocity with zero steady-state service brake when possible. To achieve this goal, velocity and service brake torques are chosen as performance variables:

$$y(k) = \begin{bmatrix} \delta v(k) & \delta T_{sb}(k) \end{bmatrix} \tag{4.13}$$

Therefore the measurement vector is:

$$C = \begin{bmatrix} 1 & 0 & 0 \\ 0 & 0 & 1 \end{bmatrix}$$

The velocity is available from the CAN. Also service brake torque can be estimated based on brake pressure measured at wheels. Therefore all the performance variables are treated as measured variables in this analysis.

The future outputs of the plant can be estimated using the above model. The disturbance, w, is assumed constant in the future horizon, if measured, and zero if unmeasured [34]. That is, if road grade is known, w is treated as measured and if the grade is unknown, w is considered unmeasured. In this work we consider both cases. The predictive equations can be written as:

$$\begin{aligned} \hat{x}(k+1|k) &= A\hat{x}(k|k-1) + B_u u(k) + B_w w(k) \\ \hat{y}(k|k-1) &= C\hat{x}(k|k-1) \end{aligned} \tag{4.14}$$

where $\hat{x}(k+1|k)$ is the estimate of the state at future sampling instant, $k+1$, based on information available at instant k, and $\hat{y}(k|k-1)$ is the output estimate at instant k based on information available at instant $k-1$. By recursive use of this equation, the future outputs $\hat{y}(k+j|k)$ can be predicted based on information available at present.

In MPC, we seek a control sequence of size N:

$$u^N = [u(k) \quad u(k+1) \quad ... \quad u(k+N-1)]^T$$

that minimizes the deviation of predicted outputs from their reference values, over the future horizon of P sampling times ($N < P$). The following finite horizon cost function is defined:

$$J = \sum_{j=1}^{P} \left(\|(r(k+j) - \hat{y}(k+j|k))\|_Q^2 + \|\Delta u(k+j-1)\|_S^2 \right) \tag{4.15}$$

where r is the reference to be tracked. The reference velocity is determined by a higher level supervisory control in automated longitudinal control [19] or by the driver in cruise control mode. The reference service brake torque is zero. The control sequence, u^N, should minimize the performance index shown above and also satisfy the compression and service brake constraints:

$$[-30 \quad 0]^T \leq u(k+j) \leq [30 \quad 5]^T \quad j = 0, 1, \ldots, N-1 \tag{4.16}$$

Furthermore we impose constraints on the rate of change of inputs, to avoid unrealistic changes. In simulations of this chapter, we used the following rate constraints:

$$[-5 \quad -0.5]^T \leq \Delta u(k+j) \leq [5 \quad 0.5]^T \quad j = 0, 1, \ldots, N-1 \tag{4.17}$$

In the performance index, S and Q are input and output weighting matrices respectively. Penalizing the change in the input, Δu, automatically adds integral action on the tracking error.

This ensures zero-steady state velocity error and zero service brake use at steady state if feasible. Predicted output, $\hat{y}(k+j|k)$, can be calculated as a function of the control sequence, u^N, only. The performance index (4.15) and the constraints (4.16) and (4.17) can be written as functions of u^N and measured outputs, disturbances and the reference command in a quadratic form. Quadratic programming techniques could be used to solve this constrained optimization problem at each sampling time. In absence of constraints, the problem reduces to a simple minimization problem and an explicit control law can be calculated. With constraints, on the other hand, a straightforward explicit control law does not exist. Instead numerical optimization of the performance index is carried out online to find the control input.[2] Simulating a constrained problem normally takes much longer time than the equivalent unconstrained problem. Since the solution depends on iterative numerical procedure, as the constraints become more stringent the computational time increases. So pushing the system to its limits for the best possible performance, might result in very large computational time. Therefore a balance between tightening the constraints and computational resources is necessary.

Selection of prediction horizon, penalty weights, and influence of mass and grade uncertainty are explained with simulation analysis, next. An adaptive scheme, which enhances the closed-loop performance is discussed in the final part of the chapter.

4.4 Simulation Results: No Adaptation

In this chapter, the closed-loop performance is studied for step deviations of the grade from the nominal point of -1.25 degrees. The desired velocity is fixed at $20m/s$. For all simulations, we used a sampling frequency of 10 Hz, which we found is sufficiently fast for this problem. We selected the length of the control horizon, N, equal to the prediction horizon, P. The length of the prediction horizon influences the stability margin and was determined in early stage of design by simulation analysis. Figure 4.1 shows loci of the closed-loop poles in the z-plane, for a particular choice of penalty weights,as the prediction horizon is increased from 2 sampling steps to 50 sampling steps. As seen in the graph, damping of the system is higher for longer horizons, at the cost of more computational time. However as seen in the figure, a prediction horizon above 10 only slightly helps the damping ratio of the poles, while, we found, noticeably increases the computation time. Therefore we fixed the prediction horizon at 10 sampling steps for the rest of simulations. Consider $Q = diag(Q_v, Q_{Tsb})$ and $S = diag(S_{ucb}, S_{usb})$ in the performance index (4.15), where Q_v, Q_{Tsb}, S_{ucb} and S_{usb} are penalties on velocity error, service brake torque, compression brake input and service brake command input, respectively. Figure 4.2 shows the influence of these weights on root mean square (RMS) velocity error and RMS service brake torque for a step change in road grade. In each plot, the x-axis shows the penalty on service brake command and each curve corresponds to a different penalty on compression brake input. Penalty on velocity error is fixed at 1 and penalty on service brake torque is set at 2×10^{-5}. The input constraints are also enforced. Based on this plot, we found that weights of 0.01 on the compression brake input and 0.1 on service brake input result in our desired closed-loop performance. Simulation with this choice of weights results in good velocity

[2]It can be shown that with linear constraints, the control is a piecewise linear function of the states. However analytical calculation of it becomes increasingly difficult as larger prediction horizons are used [39].

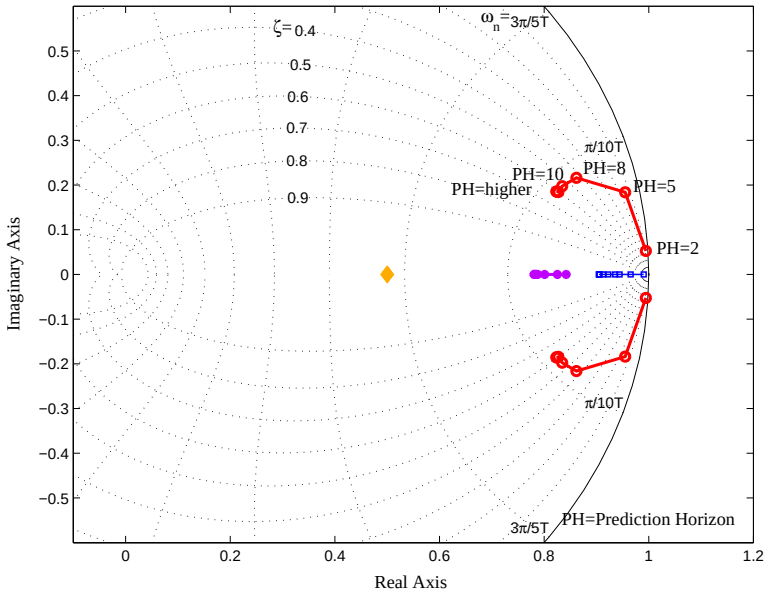

Figure 4.1: Loci of closed-loop poles in z-domain as prediction horizon increases from 2 to 50 steps. The performance index weights are $Q = diag(1, 2 \times 10^{-5})$, $S = diag(0.01, 0.1)$.

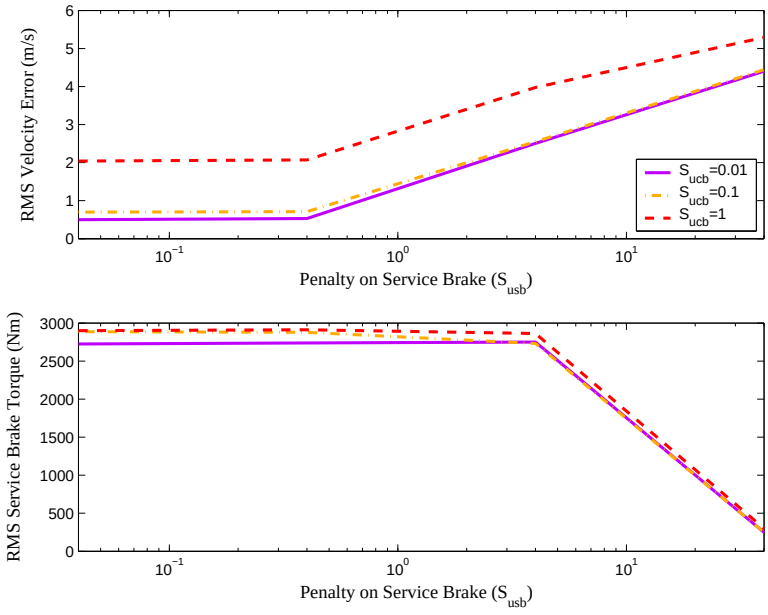

Figure 4.2: RMS error in velocity and RMS service brake torque for different penalties on each brake use. The prediction horizon is 10 sampling times.

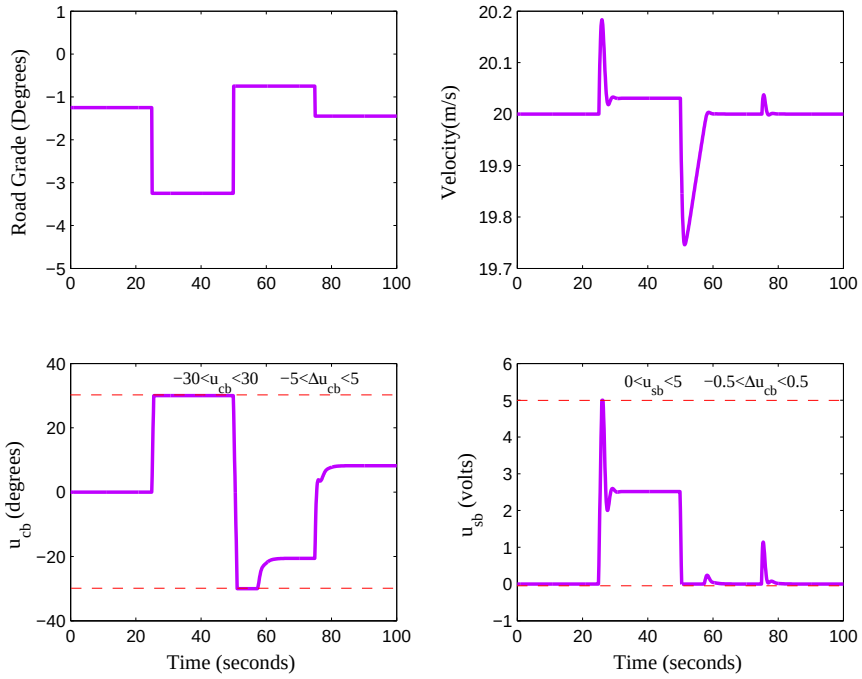

Figure 4.3: Velocity regulation with input and input rate constraints.

tracking with minimum use of service brakes as shown in figure 4.3. In this simulation we assumed that vehicle mass was known and therefore there was no discrepancy between the plant and model. Further assuming road grade is measured at each sampling time, it was used in feed-forward control. However, mass and grade are unknown in most realistic scenarios. Road grade measurement requires additional sensors which add to the cost of the vehicle. Also in heavy duty vehicles, the mass can vary largely from a configuration of no payload to full payload. Therefore a longitudinal controller that is tuned for a particular mass, might be too aggressive or too slow for a different mass. To understand the sensitivity of the closed-loop performance to such uncertainty, simulations were run for cases where mass is either underestimated or overestimated. To isolate the mass uncertainty problem, it is assumed that road grade is known.

Figure 4.4 shows simulation results when the actual vehicle mass is more than two times the modelled mass. In other words the mass is underestimated. As a result the velocity error is higher and takes longer to converge, that is the closed-loop system is slow. This can be more easily shown by comparing the closed-loop poles of this system to one in which mass is known. Figure 4.5 shows that underestimating the mass results in slower poles for closed loop system.

We observed a more critical situation when the mass of the truck is overestimated. In this scenario, as the discrepancy between the actual mass and estimated mass widens, the controller performance degrades rapidly and eventually can even result in an unstable system. Figure 4.6 shows a scenario when the controller is tuned for a fully-loaded truck and is then used to control the unloaded vehicle. Assuming large vehicle mass, the controller issues large control commands which result in oscillatory closed-loop response. Figure 4.7 compares the pole locations of the

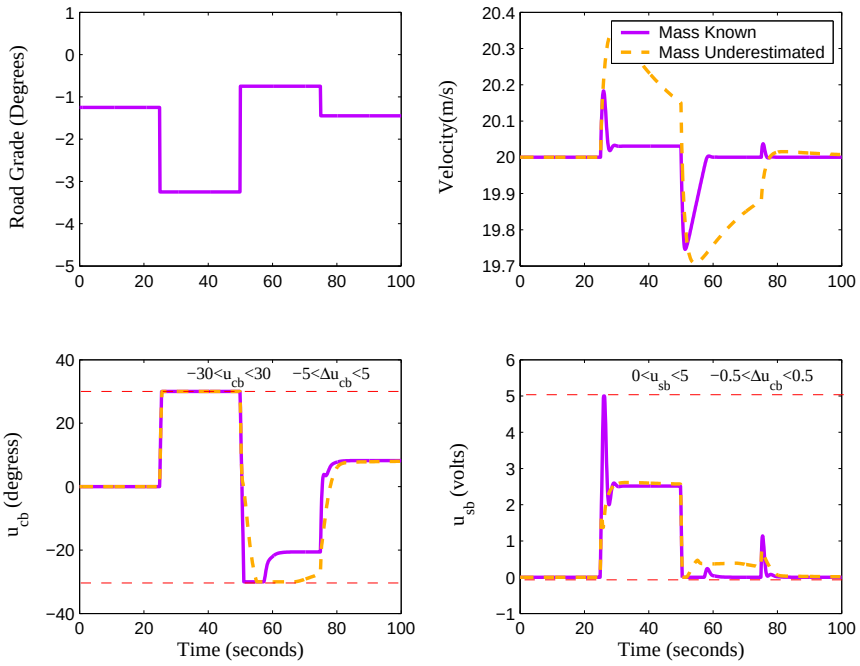

Figure 4.4: Velocity regulation when vehicle mass is underestimated.

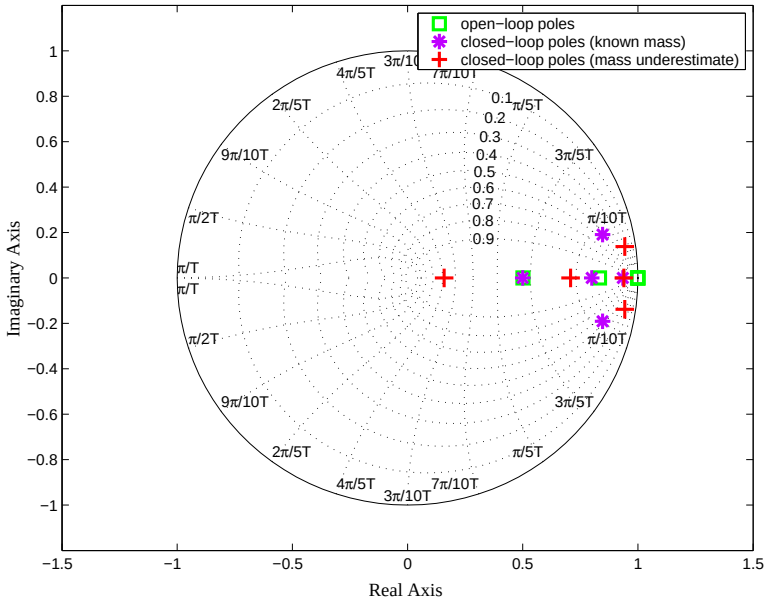

Figure 4.5: Comparison of pole locations for the open-loop and closed loop system, when mass is underestimated.

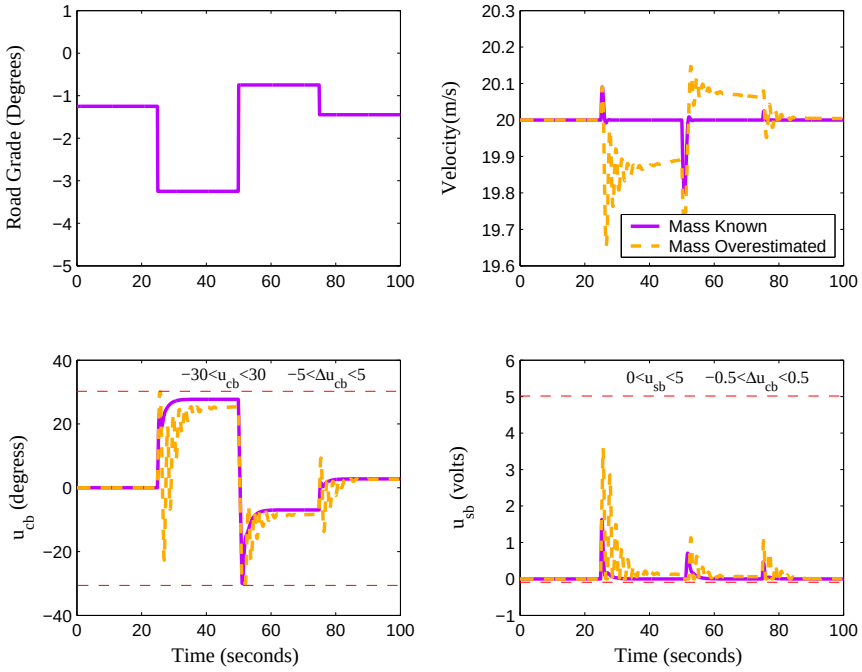

Figure 4.6: Velocity regulation when vehicle mass is overerestimated.

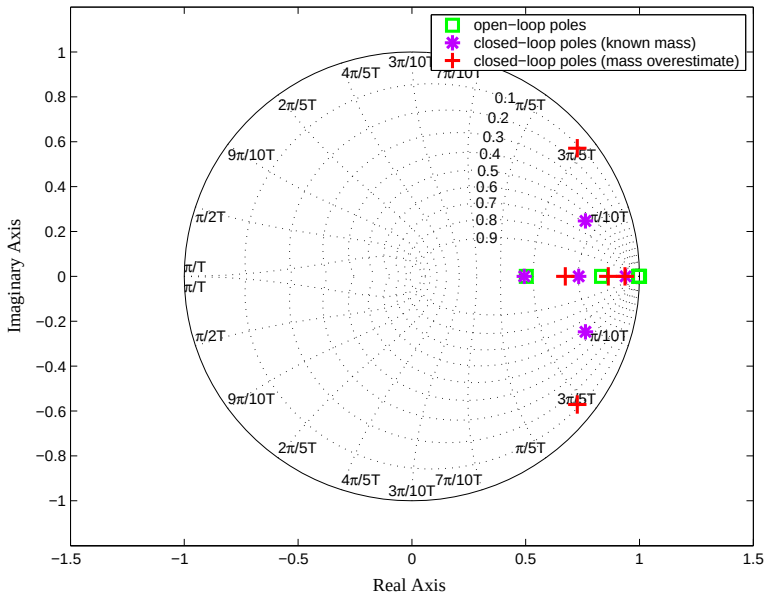

Figure 4.7: Comparison of pole locations for the open-loop and closed loop system.

closed-loop system with the case when mass is known, both unconstrained[3]. Stability margin is small when mass is overestimated as shown in this figure. When both grade and mass are unknown, the performance will degrade even further. Therefore, based on the results shown above, we think that such uncertainties can be critical to the performance and safety of a heavy vehicle. To avoid such scenarios, which limit the use of longitudinal controls, provisions need to be made in design of the speed controller. This can be done by a direct adaptive scheme which adjusts itself to parameter variations. Or mass and grade can be estimated independent of the controller and then used in an indirect adaptive control scheme. An indirect scheme has the benefit that parameter estimates can be shared with other controllers onboard the vehicle. In the next section we use an indirect adaptive controller based on the estimator developed in chapter 3 to address the short-comings of the fixed controller.

4.5 Simulation Results: With Adaptation

A recursive least square algorithm with forgetting is used for estimation of vehicle mass and road grade disturbance. Details of the estimation method are given in chapter 3. The estimation algorithm relies on the model of vehicle longitudinal dynamics and signals obtained from the vehicle CAN. The estimator is implemented in parallel with the predictive control module and updates the model at each sampling time based on the latest estimate of mass. Also the grade estimate is used for feedforward control. Our assumption is that no prior knowledge of mass or grade is available. Before initializing the recursive estimator, a batch least square estimation is performed, using some initial measurements. To ensure that level of excitations is sufficient for batch estimation, the following persistent excitation condition [3] is checked, till it is fulfilled:

$$\sum_{i=1}^{k} \left(\phi(i)\phi(i)^T\right) > \rho I_{2\times 2} \quad \rho > 0$$

The value of ρ is fixed at 0.01. This check insures that the estimation covariance matrix is not ill-conditioned and inversion does not produce meaningless results in batch estimation. After obtaining the first estimate, estimation is continued recursively using the recursive least square with vector-type forgetting explained above. The forgetting factor for grade was chosen 0.5 to keep the estimator sensitive to variations in grade. The forgetting factor for mass is chosen slightly smaller than one at 0.95. This was observed to expedite in some scenarios, convergence of mass to its actual value.

This adaptive controller tested successfully in simulations of different scenarios. Figure 4.8 shows one of the more critical cases, in which overestimation of mass and selection of aggressive penalty weights result in rapid oscillations in closed-loop response, in absence of adaptation. When the adaptive scheme is used, the performance improves noticeably, and the oscillatory behavior is reduced. Figure (4.9) shows the estimation results. Mass and grade are both estimated well, and their estimates improves as more excitation is provided to the system.

[3]The poles are calculated for the linear system without constraints, but should give an idea of behavior of the constrained system as well.

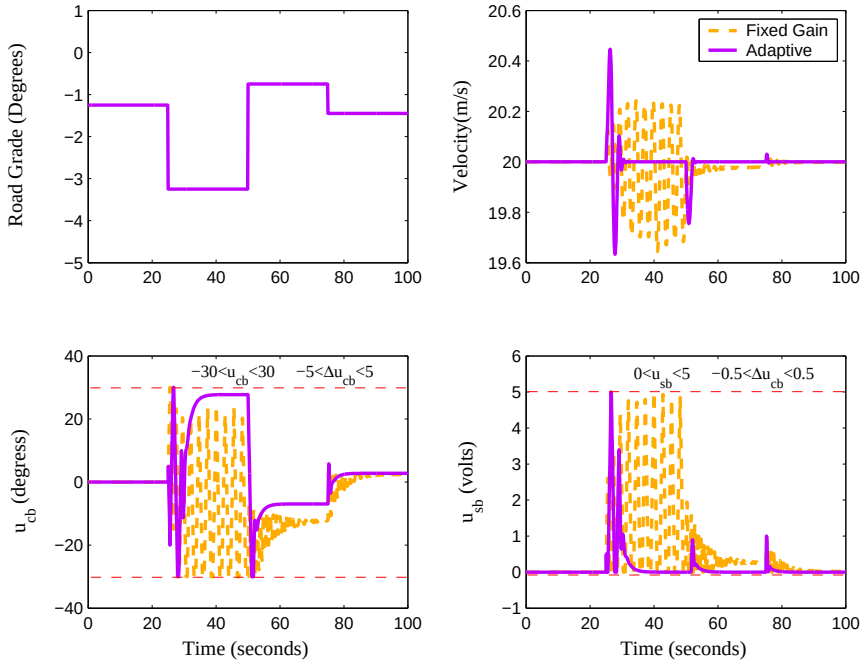

Figure 4.8: Comparison of the adaptive and fixed gain schemes when mass is overestimated.

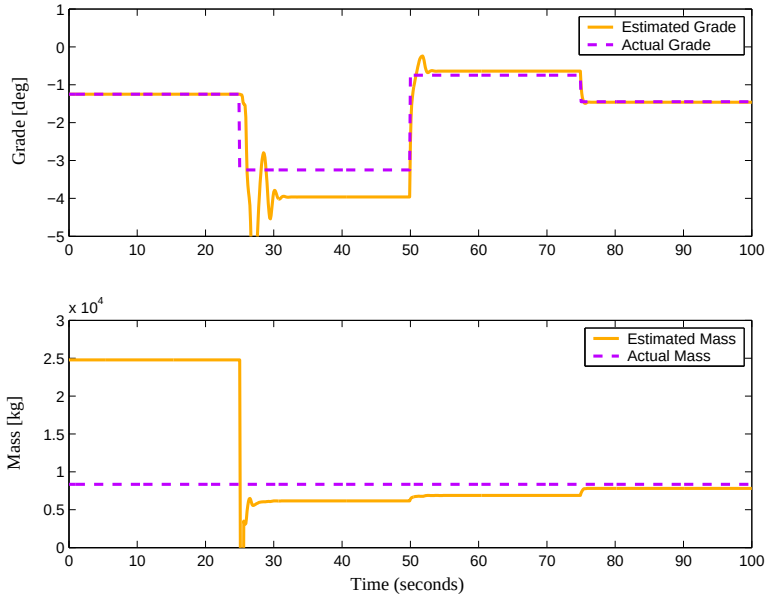

Figure 4.9: Simultaneous estimation of mass and grade, when mass is overestimated. Forgetting factors are 0.95 and 0.5 for mass and grade respectively.

4.6 Conclusions

In this chapter, an adaptive model predictive control scheme is designed for speed control of heavy vehicles. The longitudinal control of vehicles is traditionally addressed by classical control techniques such as PI control. Nonlinear techniques like sliding mode control have been used to handle nonlinearities of components like engine and brake dynamics and adaptive control techniques have previously been studied for handling uncertainties. However formulation in an optimal control framework has not been investigated as much. In this chapter we formulated the linearized dynamics of the engine brake, service brakes and powertrain in state space and demonstrated subsequently that model predictive control could be used for reference velocity tracking. The controller coordinates use of compression brakes and service brakes on downhill slopes. The use of service brake was minimized by penalizing its steady-state use. Given a perfect model, good performance was obtained in closed-loop. We showed with simulation analysis that model uncertainties due to uncertainty in vehicle mass result in degraded and sometimes very poor oscillatory closed-loop response. Unknown road disturbance (grade) was another limiting factor to the performance of the controller.

To rectify such problems, a recursive least square scheme with forgetting factor was used in an indirect adaptive scheme. The estimation scheme runs in parallel with the controller and updates the model at each step based on the new estimate of mass. Grade estimates are also used in feedforward control. The estimator and controller both converged very well and resulted in remarkable improvements in closed-loop performance. Adding grade estimates in feedforward control contributed to much quicker regulation of velocity.

Bibliography

[1] *Recommended Practice for a Serial Control and Communications Vehicle Network*. Society of Automotive Engineers, 1998.

[2] *Surface Vehicle Recommended Practice; Vehicle Application Layer*. Society of Automotive Engineers, 1998.

[3] A. Astrom and B. Wittenmark. *Adaptive Control*. Addison Wesley, second edition, 1994.

[4] H.S. Bae and J. Gerdes. Parameter estimation and command modification for longitudinal control of heavy vehicles. *Proc. of International Symposium on Advanced Vehicle Control*, 2000.

[5] H.S. Bae, J. Ryu, and J. Gerdes. Road grade and vehicle parameter estimation for longitudinal control using GPS. *Proc.of IEEE Conference on Intelligent Transportation Systems*, 2001.

[6] S. Bittani, P. Bolzern, and M. Campi. Convergence and exponential convergence of identification algorithms with directional forgetting factor. *Automatica*, 26, 5:929–932, 1990.

[7] S. Bittani, P. Bolzern, M. Campi, and E. Coletti. Deterministic convergence analysis of RLS estimators with different forgetting factors. *Proceedings of the 27th Conference on Decision and Control*, pages 1530–1531, 1988.

[8] A.E. Bryson and Y.C. Ho. *Applied Optimal Control: Optimization, Estimation, and Control*. Hemisphere Publishing, New York, 1975.

[9] Marco Campi. Performance of RLS identification algorithms with forgetting factor: A Phi-mixing approach. *Journal of Mathematical Systems, Estimation and Control*, 4, 3:1–25, 1994.

[10] Liyu Cao and Howard M. Schwartz. A novel recursive algorithm for directional forgetting. *Proceedings of the American Control Conference*, pages 1334–1338, 1999.

[11] M. Druzhinina, L. Moklegaard, and A. Stefanopoulou. Speed gradient approach to longitudinal control of heavy-duty vehicles equipped with variable compression brake. *IEEE Transactions on Control Systems Technology*, 10:209–220, 2001.

[12] M. Druzhinina, A. Stefanopoulou, and L. Moklegaard. Adaptive continuously variable compression braking control for heavy-duty vehicles. *ASME Dynamic Systems, Measurement and Control*, 124:406–414, 2002.

[13] Maria Druzhinina and Anna Stefanopoulou. Speed control experiments for commercial heavy vehicles with coordinated friction and engine compression brakes. *Proc. of American Control Conference*, 2002.

[14] T.R. Fortescue, L.S. Kershenbaum, and B.E. Ydstie. Implementation of self-tuning regulators with variable forgetting factors. *Automatica*, 17, 6:831–835, 1981.

[15] Thomas A. Genise. Control method system including determination of an updated value indicative of gross combination weight of vehicles. *US Patent No 5,490,063*, 1994.

[16] T. Hagglund. Recursive estimation of slowly time-varying parameters. *Proceedings of IFAC*, pages 1137–1142, 1985.

[17] P. Ioannou and Z. Xu. Throttle and brake control systems for automatic vehicle following. *PATH Research Report UCB-ITS-PRR-94-10*, 1994.

[18] C.R. Johnson. *Lectures on Adaptive Parameter Estimation*. Prentice Hall, 1988.

[19] S. Joo, X.Y. Lu, and J.K Hedrick. Longitudinal maneuver design in coordination layer for automated highway system. *Proceedings of American Control Conference*, pages 42–47, 2003.

[20] R. Kulhavy. Restricted exponential forgetting in real-time identification. *Proceedings of IFAC*, pages 1143–1148, 1985.

[21] R. Kulhavy and M.B. Zarrop. On a general concept of forgetting. *International Journal of Control*, 58, 4:905–924, 1993.

[22] J.H. Lee and N.L. Ricker. Extended kalman filter based nonlinear model predictive control. *Industrial and Engineering Chemistry Research*, 33:1530–1541, 1994.

[23] M.K. Liubakka, D.S. Rhode, J.R. Winkelman, and P.V. Kokotovic. Adaptive automotive speed control. *IEEE Transactions on Automatic Control*, 38, 7:146–156, 1993.

[24] Lennart Ljung and Svante Gunnarsoon. Adaptation, tracking and system identification - a survey. *Automatica*, 26,1:7–21, 1990.

[25] Xiao-Yun Lu and Karl Hedrick. Longitudinal control design and experiment for heavy-duty trucks. *Proceedings of the American Control Conference*, pages 36–41, 2003.

[26] Jan Marian Maciejowski. *Predictive Control with Constraints*. Prentice Hall, Essex, England, 2002.

[27] L. Moklegaard, A.G. Stefanopoulou, and J. Schmidt. Transition from combustion to variable compression braking. *SAE Paper No 2000-01-1228*, 2000.

[28] Lasse Moklegaard, Maria Druzhinina, and Anna Stefanopoulou. Compression braking for longitudinal control of commercial heavy vehicles. Technical Report UCB-ITS-PRR-2001-11, PATH, 2001.

[29] Lasse Moklegaard, Maria Druzhinina, and Anna Stefanopoulouler. Longitudinal control of commercial heavy vehicles with variable compression brake. *Technical Report TO 4200,PATH*, 2001.

[30] K. Oda, H. Takeuchi, M. Tsujii, and M. Ohba. Practical estimator for self-tuning automotive cruise control. *Proceedings of the American Control Conference*, pages 2066–2071, 1991.

[31] H. Ohnishi, J. Ishii, M. Kayano, and H. Katayama. A study on road slope estimation for automatic transmission control. *JSAE Review*, 21:322–327, 2000.

[32] J.E. Parkum, N.K. Poulsen, and J. Holst. Selective forgetting in adaptive procedures. *Proceedings of the 11th Triennial World Congress of the IFAC*, 2:137–142, 1990.

[33] J.E. Parkum, N.K. Poulsen, and J. Holst. Recursive forgetting algorithms. *International Journal of Control*, 55, 1:109–128, 1992.

[34] N.L. Ricker. Model predictive control with state estimation. *Industrial and Engineering Chemistry Research*, 29:374–382, 1990.

[35] Steiner Saelid, Olav Egeland, and Bjarne Foss. A solution to the blow-up problem in adaptive controllers. *Modeling, Identification and Control*, 6, 1:36–39, 1985.

[36] Steiner Saelid and Bjarne Foss. Adaptive controllers with a vector variable forgetting factor. *Proceedings of the 22nd IEEE Conference on Decision and Control*, pages 1488–1494, 1983.

[37] Mario E. Salgado, Graham C. Goodwin, and H. Middleton Richard. Modified least squares algorithm incorporating exponential resetting and forgetting. *International Journal of Control*, 47, 2:477–491, 1988.

[38] N. Rao Sripada and D. Grant Fisher. Improved least square identification. *International Journal of Control*, 46, 6:1889–1913, 1987.

[39] P. Tondel, T. Johansen, and A. Bemporad. An algorithm for multi-parametric quadratic programming and explicit MPC solutions. *Automatica*, 39(3):489–497, March 2003.

[40] Ardalan Vahidi, Anna Stefanopoulou, and Huei Peng. Recursive least squares with forgetting for online estimation of vehicle mass and road grade: Theory and experiments. *To appear in Journal of Vehicle System Dynamics*, 2004.

[41] Ardalan Vahidi, Anna G. Stefanopoulou, Phil Farias, and Tsu-Chin Tsao. Experimental verification of discretely variable compression braking control for heavy duty vehicles. *PATH Annual Report*, 2003.

[42] J.Y. Wong. *Theory of ground Vehicles*. John Wiley and Sons, third edition, 2001.

[43] M. Wuertenberger, S. Germann, , and R. Isermann. Modelling and parameter estimation of nonlinear vehicle dynamics. *Proceedings of ASME Dynamical Systems and Control Division*, 44, 1992.

[44] D. Yanakiev, J. Eyre, and I. Kanellakopoulos. Longitudinal control of HDV's: Experimental evaluation. Technical Report MOU 293, PATH, 1998.

[45] D. Yanakiev and I. Kanellakopoulos. Speed tracking and vehicle follower control design for heavy-duty vehicles. *Vehicle System Dynamics*, 25:251–276, 1996.

[46] D. Yanakiev and I. Kanellakopoulos. Longitudinal control of automated CHV's with significant actuator delays. *Proceedings of 36th IEEE Conference on Decision and Control*, 1997.

[47] Naoharu Yoshitani and Akihiko Hasegawa. Model-based control of strip temperature for the heating furnace in continuous annealing. *IEEE Transactions on Control Systems Technology*, 6, 2:146–156, 1998.